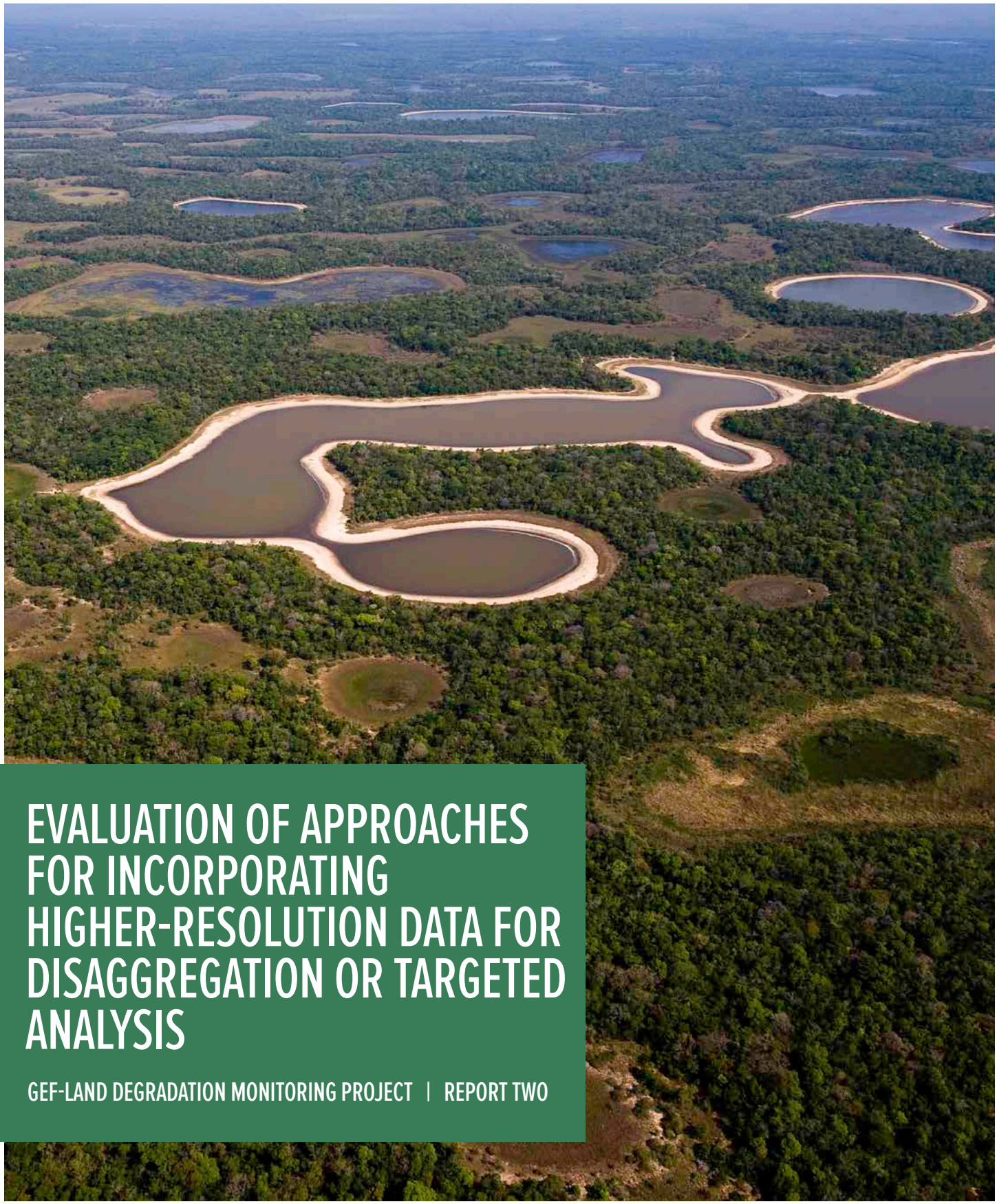

EVALUATION OF APPROACHES FOR INCORPORATING HIGHER-RESOLUTION DATA FOR DISAGGREGATION OR TARGETED ANALYSIS

GEF-LAND DEGRADATION MONITORING PROJECT | REPORT TWO

CONSERVATION INTERNATIONAL

gef
GLOBAL ENVIRONMENT FACILITY
INVESTING IN OUR PLANET

VITAL SIGNS

LUND UNIVERSITY

NASA

Evaluation of approaches for incorporating higher-resolution data for disaggregation or targeted analysis

GEF-Land Degradation Monitoring Project
Report Two

Jorge E. Pinzon, Katherine Melocik, Erin Glennie, Jennifer Small, Claire Porter, and Compton J. Tucker

This report was produced as an output of the Global Environment Facility (GEF)-funded project "Enabling the use of global data sources to assess and monitor land degradation at multiple scales". The project aims to provide guidance on robust methods and a toolbox for assessing and monitoring status of land degradation using remote sensing technology.

For additional information on the project see http://vitalsigns.org/gef-ldmp.

The Land Degradation Monitoring Project is a collaboration of Conservation International, Vital Signs, the National Aeronautics and Space Administration (NASA), and Lund University.

TABLE OF CONTENTS

I. INTRODUCTION

1. INTRODUCTION

Our previous report (Tucker and Pinzon 2017) showed that coarse spatial resolution of long-term NDVI datasets at 250 m (17+ years) to 8 km (35+ years) are a key technology for long-term monitoring of vegetation productivity. The longevity of the record and its routine global coverage enabled us to separate and reveal trends in primary productivity that are independent of many natural fluctuations of climate variables affecting vegetation such as prolonged drought. These trends could be used as proxies of land degradation. Useful as this record is, the coarse resolution of these sensors, however, imposes key challenges since it limits our ability to identify attribution and separation of the effects of changes. For instance, from studies of dryland savannas using coarse resolution long-term time series, it is known that annual herbaceous vegetation contribute to most of the inter-annual variability, while the woody strata contribute more to long-term trends (Fensholt *et al*. 2012; Gonzalez *et al*. 2012). However, the magnitude of their contribution and their spatial patterns are not well characterized in these studies since the spatial resolution inhibits the detection of scattered canopies of bushes, shrubs, and small trees typical of dryland savannas like the Sahel (Gonzalez *et al*. 2012; Brandt *et al*. 2016; Rishmawi *et al*. 2016).

In this report, we review higher-resolution data sources, evaluate their suitability and trade-offs for land degradation monitoring (e.g. cost of use, resolution, accessibility, repeatability, sustainability, and potential for automated analysis), and review approaches to disaggregate indicators for degradation or other changes detected from coarser spatial resolution data to medium and fine resolutions (sections I.1 and I.2). This review resulted in a proposed algorithm to conduct aggregation and disaggregation via data merging (section II). Finally, we described the final remote sensing methodology to combine high temporal but coarser spatial resolution data with finer spatial resolution data for assessing land degradation (section III).

In contrast to the high temporal but coarse spatial resolution data, medium (e.g. Landsat with 30 m spatial resolution) to fine-resolution (commercial satellite Very High Resolution (VHR) data with 5 m-0.5 m spatial resolution) imagery is well suited for characterizing structure and patterns at landscape-level vegetation (Cohen and Goward 2004; Coops *et al*. 2006; Roy *et al*. 2008; Wulder *et al*. 2008). Typically, these higher spatial resolution data result in a smaller spatial extent (image footprint) and a lower revisit rate (e.g. for Landsat data revisit time is 16 days). When considering that cloud cover may impact any given acquisition, the revisit cycle can be significantly longer, limiting their use for monitoring vegetation dynamics (Cohen and Goward, 2004; Coops *et al*. 2006). An ideal for satellite vegetation monitoring would be to have both high spatial and temporal resolutions. In this study, we review methods on the usage of medium to fine spatial resolution data that provide sufficiently detailed information to attribute the proximate causes of changes detected with long-term high temporal resolution data.

Some of the basic questions that arise from these experiments, illustrate a typical situation encountered when solving what is known as inverse problems, that is, when we want to obtain information of the internal structure of the physical (local) vegetation system from the vegetation dynamics provided by the course resolution and medium-high resolution data. Here, we build our approach in terms of an inverse problem perspective, and investigate ways to combine high spatial resolution with high temporal resolution data to capitalize on the spatial detail and the temporal regularity of acquisitions and provide enough spatial detail to identify attribution and separation of the effects of changes, and thus improve interpretation of trends, e.g. the kind of degradation or drivers.

I.1. BACKGROUND ON USAGE OF HIGH RESOLUTION DATA IN MAPPING LAND DEGRADATION

In general, high spatial resolution data are helpful for fine-scale assessments and analysis at local scales (Gonzalez *et al*. 2012; Brandt *et al*. 2016) while medium spatial resolution data are useful at regional or higher scales (Cohen and Goward 2004; Coops *et al*. 2006; Roy *et al*. 2008; Wulder *et al*. 2008). At a continental or global scale, coarse spatial resolution data support archives of long time series that provide both inter-annual and seasonal information and they are preferred for many NDVI-based assessments and analyses. In fact, long time series allow for the use of remote sensing to assess land degradation and monitor changes (Symeonakis and Drake 2004; Shalaby and Tateishi 2007; de Jong *et al*. 2011; Anyamba and Tucker 2012; Townshend *et al*. 2012; Albalawi and Kumar 2013; Rishmawi *et al*. 2016).

The opening of free United States Geological Survey (USGS) Landsat archive in 2008 (Woodcock *et al*. 2008) ushered in a new era of applications and wider uses of Landsat data and more recently very high-resolution (VHR) commercial data. The result is a more accurate and reliable spatial analysis over large areas and an improvement in the quality of decisions based on these data (Masek *et al*. 2016). Since then, the new focus has been on leveraging the time domain for inter-annual disturbance, land degradation, land use changes, and vegetation gross primary production. There are numerous examples in the literature that combine data from sensors with similar medium spatial resolution and harmonize them to provide long-term high frequency monitoring applications (Mandacini, 2016; Masek *et al*. 2016).

Other examples combine data from sensors with differing spatial, spectral and temporal characteristics to improve spatial mapping and interpretation of trends (Tucker & Townshend 2000; Gonzalez *et al*. 2012; Yavasli *et al*. 2015; Brandt *et al*. 2016), enhance the spatial resolution of the spectral

Tea plantations in eastern Rwanda. © Levi S. Norton

data (Carper *et al*. 1990; Yocky 1996; Pohl and Genderen 1998; Hilker *et al*. 2009; Sedano *et al*. 2014), predict temporal changes in reflectance in the higher spatial resolution data, e.g. Landsat, using high temporal frequency data but Moderate Spatial Resolution Imaging Spectroradiometer (MODIS), and generate a synthetic Landsat time series to investigate vegetation dynamics at 30 m Landsat resolution of different land cover types (Gao *et al*. 2006; Roy *et al*. 2008; Hansen *et al*. 2008; Hilker *et al*. 2009; Sedano *et al*. 2014).

European Space Agency's (ESA) Sentinel-2a and Sentinel-2b, both with a 20 m spatial resolution, and National Aeronautics and Space Administrations' (NASA) Landsat-8's 30 m products, arguably are the most widely accessible medium spatial resolution multispectral satellite data. These datasets create opportunities for a synergistic use of the two sources for timely and accurate observation of Earth status and dynamics at the 30 m scale (Hilker *et al*. 2009; Sedano *et al*. 2014). In addition, incorporation of 30-50 cm commercial satellite data is of fundamental importance for the scientific community for improved mapping and interpretations of land degradation trends and for identification of pressures or possibly drivers. Monitoring patch-scale vegetation dynamics, particularly for degraded and agricultural regions, requires both fine spatial resolution and at least an 8-day temporal frequency. While this is a very difficult task for a single medium to high-resolution sensor such as Landsat, harmonizing multiple international sources of data can provide a cost-effective pathway to fine spatial resolution and high temporal Earth monitoring capability. NASA, the USGS, and ESA have started a collaboration to develop a processing chain that creates seamless, "harmonized" reflectance products from combined Landsat, Sentinel-2a, and Sentinel-2b observations.

The "harmonization" approach uses standardized atmospheric correction, bidirectional reflectance distribution function (BRDF) adjustment, spectral band-pass adjustment, and gridding algorithms to guarantee same geophysical measurements, taking advantage that both sensors are similar in terms of spectral and spatial measurements.

These products point the way to a "30 m MODIS" capability for agricultural, ecosystem monitoring and land degradation monitoring by leveraging international sensors. When combined, observations from both sensors can provide 2-4 day coverage for global land areas (Mandacini, 2016; Masek *et al*. 2016).

Image fusion from different sensors requires a well-defined technique as well as a good understanding of the input data (Pohl and Genderen 1998, Hilker *et al*. 2009). Since we aim to capitalize on the spatial detail provided by VHR commercial data to improve spatial mapping and interpretation of the temporal trends, we add VHR spatial information to normalized NDVI Landsat imagery and resolve the characteristics of the 0.5 m 3600 (60x60) elements that makes a 30 m Landsat pixel, i.e. we exploit a simple pan-sharpen fusion technique to improve landscape discrimination.

I.2. EVALUATION OF AVAILABLE HIGH RESOLUTION DATA SOURCES THAT CAN BE USED FOR DISAGGREGATION

We are producing commercial satellite data mosaics for all of Senegal, Uganda, Kenya and Tanzania for better characterization of land-cover and land-use mapping with Landsat-8 and Sentinel-2a data (Figure 1, see Appendix A for a description of the process creating VHR mosaics). These detailed data have never been used previously in this region at this large a spatial extent to identify land degradation, or to determine the cause(s) of the land degradation, and will enable remedies to be undertaken to reverse land degradation (See Table 1, page 10-11).

For this study, through the involvement of Tucker and his team at the NASA Goddard Space Flight Center (GSFC), we are able to access thousands of commercial satellite images with <20% cloud cover for Kenya, Senegal, Tanzania, and Uganda for the time period of 2002-2016. Our land degradation study is exactly the type of NASA research project for which NGA hopes NASA will use these data.

TABLE 1

DATA SOURCE	SPATIAL RESOLUTION(S)	EQUATORIAL TEMPORAL FREQUENCY	USE	ANALYTICAL APPROACHES AND EXPECTED OUTCOMES	COST
LANDSAT-5 (THEMATIC MAPPER) TM **LANDSAT-7 (ENHANCED TM PLUS) ETM+**	30 m	16 days with longer cycles when cloud clover	Confirmation of land degradation from 1982 using Landsat-5 and Landsat-7 data to 2015	30 m disaggregation of AVHRR and MODIS data to sub-national and community scales	Free and distribute by tiles. The Landsat 7 ETM+ products have along scan stripes of missing data due to scan line corrector that failed in 2003. It reduces the usable data in each ETM+ scene by about 22% (Markham *et al*. 2004)
LANDSAT-8 **OLI**	30 m	3.7 days now with combined Sentinel-2a and Sentinel-2b data	Confirmation of land degradation from 2000 using Landsat-7 data to 2015 and beyond with Landsat-8 and -9 data	Combination of Landsat-8 and ESA Sentinel-2a and -2b observations will provide <4 day coverage for global land areas	Free and distribute by tiles
SENTINEL-2A AND -2B	20 m	3.7 days now with combined Landsat-8; 3 days in 2020 when Landsat-9 joins the team	Confirmation of land degradation from 2016 and 2017 and into the 2020s	Combined with Landsat data for 2016-2017 (data start in 2016 will provide <4 day coverage for global land areas	Free and distribute by tiles
DIGITALGLOBE COMMERCIAL SATELLITES (QUICKBIRD-2, WORLDVIEW-1, WORLDVIEW-2, GEOEYE-1)	2.4 m (multispectral) 0.5 m (Panchromatic) imagery	Coverage every 1-3 years. Theoretical frequency is around 1-3.5 days depending on latitude, but smaller spatial extent increases sensor's revisit rate	Local-scale confirmation of land degradation from 2002-2017 and beyond	Land degradation disaggregation to 30, 40, & 50 cm to understand drivers & processes at local level or used to validate vegetation features extracted from medium spatial resolution imagery	$14 for sq. km (with a minimum order area of 25 sq. km for archive imagery) http://www.landinfo.com/satellite-imagery-pricing.html (last accessed 8/17/17)* Basic codes M1B5, M4AM, P1B5, and P4AM

CONTINUED

DATA SOURCE	SPATIAL RESOLUTION(S)	EQUATORIAL TEMPORAL FREQUENCY	USE	ANALYTICAL APPROACHES AND EXPECTED OUTCOMES	COST
PLANET SCOPE	3 m (4 band multispectral: RGB, NIR)	Revisit time 1 day	Satellites can collect 5 million km2 daily	16 bit for analysis and 8 bit for visual	Cost quote depends on order requirements
SKYSAT	0.9 m (Panchromatic)2m (multispectral)	Revisit time 3-5 days	Data back to Jan 2014 and more frequent after SkySar-2 launched on July 2014.	Smallest satellite flown capable to capture 1m resolution data	Cost quote depends on order requirements
RAPIDEYE	5 m (5 band multispectral: RGB, red edge, NIR)	Revisit time 1 day	Satellites can collect 5 million km2 daily	Five Earth imaging satellites with identical sensors for more frequent analysis	Cost quote depends on order requirements
AIRBUS DEFENSE & SPACE IMAGERY PRODUCTS (SPOT 5, SPOT 6/7, PLEIADES)	1.5 m-10 m SPOT (multispectral, PAN) 0.5 m (PAN) 2 m (RGB, NIR)	Revisit time 1-3 days	Holds one of the world's largest continually growing High resolution image libraries back to 1986.	Useful for large and small scale mapping.	Cost quote depends on order requirements

Table 1. Sources of higher spatial resolution satellite data, their uses, and their analytical approaches and expected outcomes. The "harmonized" Landsat-8/Sentinel-2a/Sentinel-2b multi-spectral 30 m data have an equatorial revisit frequency of 3.7 days now. When Landsat-9 joins the team in 2020, the equatorial revisit frequency will drop to 3.0 days. *Commercial data: The National Aeronautics and Space Administration (NASA) has an agreement with the National Geospatial Intelligence Agency (NGA) to access NGA-purchased commercial satellite data at no cost for use in conjunction with NASA research projects. NASA GSFC has already acquired commercial satellite data over much of sub-Saharan Africa, the four pilot countries and other parts of the world.

While NASA cannot provide copies of the raw commercial satellite data to others, it can distribute derived products from them if they cannot be used to re-create the original data. Updated guidelines on NextView Licensed imagery state that geo-referenced images are allowed to be distributed, however no publicly released imagery can be reverse engineered to obtain the original image values, and each image must have a copyright burned into it. To ensure conformance with NextView's requirements, it was decided in meetings with Conservation International (CI) to use geo-referenced "lossy" JPEG's as the distribution format.

The commercial high-resolution mosaic code was originally created by the University of Minnesota's Polar Geospatial Center (PGC) and recently improved at NASA/GSFC. The code corrects for terrain and radiometry, mosaics several images into one set of tiles, and pan-sharpens multispectral images with its panchromatic partner. Two separate mosaic codes are currently in use, one for panchromatic data only and one for NDVI/ PAN data. Mosaic tiles are with a WGS84/ UTM zone specific projection. Due to differences in satellite resolution, all mosaics are resampled to 50 cm. We have organized the 50 cm spatial resolution commercial satellite imagery into 100 x 100 km blocks at 25 x 25 km GeoTIFF sub-tiles for both the panchromatic and our multi-spectral imagery. For efficient runs, the mosaic code only included imagery with basic levels of image processing from DigitialGlobe, i.e. multispectral product codes M1BS and M4AM as well as panchromatic product codes P1BS and P4AM (see Appendix A for more details).

At the start of this project, some commercial high-resolution imagery was already obtained over the four pilot countries; however, NASA did not have all available images. Thus, our inventory differed with DigitalGlobe's available imagery and the complementary data was ordered. To ensure we get the best results, we continue to update our inventory whenever DigitalGlobe releases new imagery.

Ordered data are comprised of imagery from the following DigitalGlobe satellites: GeoEye-1, QuickBird-2, WorldView-1, and WorldView-2. Imagery contains 20% cloud cover or less and includes all years and months.

Commercial high-resolution data acquisition started as early as March 2015 over the project areas. From early 2015 until present, regular order updates have been assembled, processed, and submitted. As of April 24, 2017, NASA has acquired all 188,409 images that are available within the NASA Center for Climate Simulations (NCCS) archive over the four pilot countries from DigitalGlobe satellites to complete all 267 NDVI/Panchromatic mosaic tiles (Figure 1). Both multispectral and panchromatic images were obtained and 50 cm resolution mosaics over pilot countries were created (Figure A1 and Figure A3).

The data are of sufficiently high resolution to reveal up to individual trees and bushes. The GSFC team is currently researching automated approaches to detect crowns, and thus characterize varying tree and shrub density over large areas. In some areas, high-resolution data are available over a multiple-year period, revealing patterns of agricultural abandonment, savanna clearing to expand cropped lands or to respond to increasing demand for charcoal and wood-fuel, vegetation recovery, and other patterns of land-use change in fine detail. However, the archive for these data is not as comprehensive as the Landsat or MODIS archives, and it mostly extends back only to 2002. Most coarse scale studies imply that the degradation trends are influenced by climate patterns and human activities, but by adding finer-resolution data, we can examine more precisely what has occurred in particular places that show unique trend signals. They can also be used to compare approaches and to calibrate and validate relationships between the coarser data and the occurrence of degradation or improvement.

However, capacity in many countries for use of such data is very limited. Capacity development needs can be grouped into three categories: knowledge capacity, financial capacity and logistical capacity. Both financial and logistical capacity can be addressed by providing a method that uses derived products with demonstrated relationships to degradation and other changes, yet are relatively simple and not large in data volume.

Providing derived products over large regions or over a requested set of countries would also reduce potential for inconsistent application of methods among countries. The fusion of VHR imagery with multiple Landsat imagery should help to mitigate further the risk of both financial and logistical capacity. Thus, the VHR commercial satellite data, when used together with Landsat, MODIS, and AVHRR data, represent an excellent combined resource for evaluating land degradation and for guiding remediation efforts to reverse land degradation.

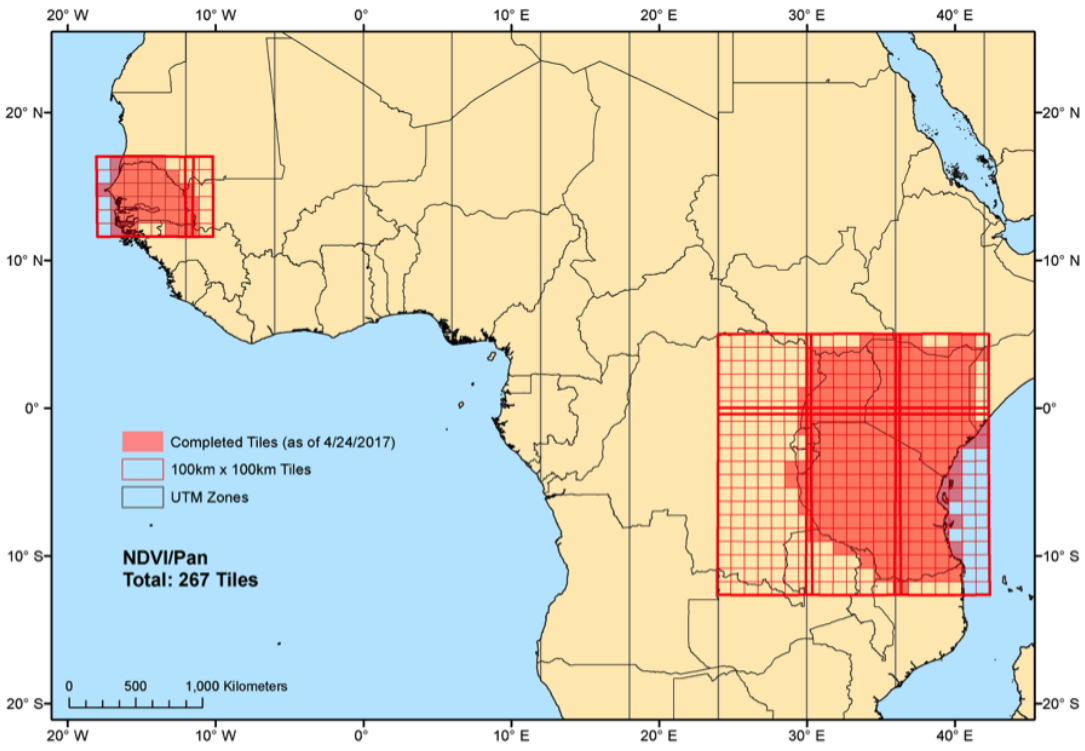

Figure 1. DigitalGlobe 50 cm resolution panchromatic and multi-spectral imagery in our archive over pilot countries, Senegal (45,713 images), Uganda (26,028 images), Kenya (39,674 images) and Tanzania (76,994 images). All data are <20% cloud cover and available for our land degradation study.

Figure 2 shows the yearly distribution of the cutline images available for all four pilot countries. Notice that each country has more than 1000 images after 2010 since Worldview1-2 started to contribute additional imagery to the archive in 2007. Similarly, Figure 3 shows the monthly distribution of the VHR imagery. These data will be invaluable for developing a highly detailed mapping of land cover and land use changes that would have explicit uses for identifying land degradation and its drivers. The frequency distribution of images throughout the year is biased towards November-February, potentially affecting and biasing the selection of images that go into the mosaics towards the months with higher density of available data.

For Senegal, it will mostly emphasize the dry periods (where high density of cloud-free imagery is expected). However, few images representing the growing season (July-September) would be selected. This bias towards dry periods in Senegal would have the tendency to highlight the spatial features where low NDVI is expected. For Tanzania, the peak of image distribution during November-February coincides with rainy periods and thus, images with cloud cover greater >20% are expected. That makes difficult the task of the selecting cloud-free images for the mosaics. We do not expect such problems for Kenya and Uganda since dry seasons (with light rain) are from December to February and June to August.

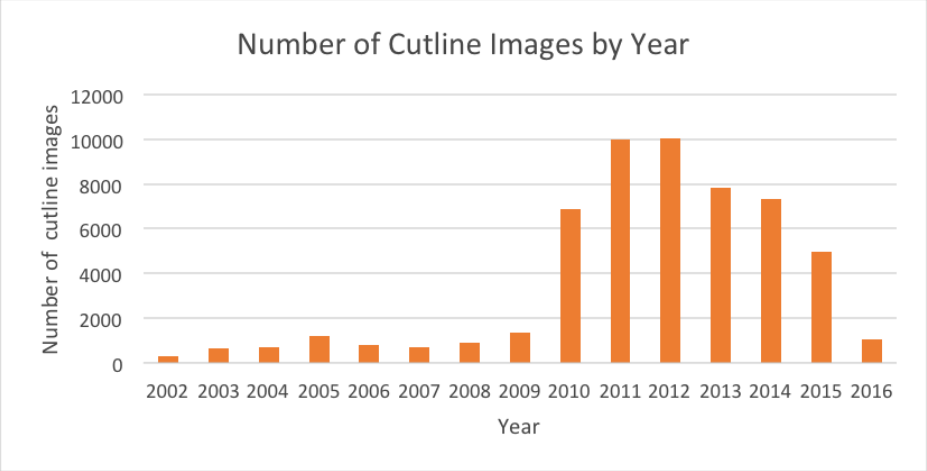

Figure 2. Distribution of VHR (NDVI/PAN mosaic) imagery for all four pilot countries by year. The same patterns are observed for each of the four pilot countries. Images as of 04/27/2017 and basic product codes M1BS and M4AM for multispectral imagery as well as basic product codes P1BS and P4AM for panchromatic imagery.

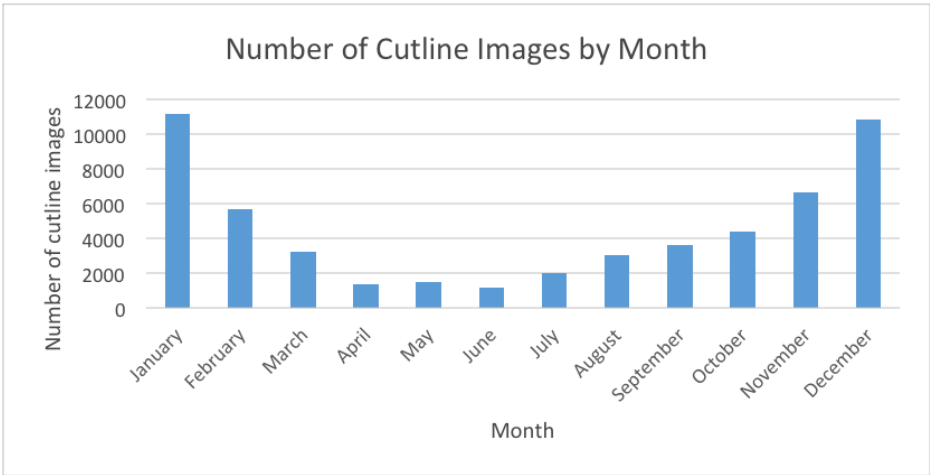

Figure 3. Distribution of VHR (NDVI/PAN mosaic) imagery for all pilot countries by month. Images as of 04/27/2017 and basic product codes M1BS and M4AM for multispectral imagery as well as basic product codes P1BS and P4AM for panchromatic imagery.

II. APPROACHES TO DISAGGREGATE LAND DEGRADATION INDICATORS

II.1. INTRODUCTION

Since 2000, an improved generation of moderate- and coarse-resolution instruments, such as SPOT-VEGETATION, Medium Resolution Imaging Spectrometer (MERIS) and Moderate Resolution Imaging Spectroradiometer (MODIS), has enhanced our capabilities for monitoring vegetation dynamics. These new data capabilities, combined with the opening of the Landsat archive (Woodcock *et al*. 2008), create opportunities for extending temporal studies to higher spatial resolutions.

However, the potential for continuous monitoring of land processes is limited due to the Landsat 16 day revisiting period and the availability of cloud-free surface observations. A common practice to overcome this limitation is to provide snapshots of a given epoch (Hansen *et al*. 2008) but this won't be a truly continuous monitoring with medium spatial resolution data. Thus, the idea of filling the temporal gaps with synthetic Landsat time series obtained through the combination of high temporal moderate- and medium-spatial resolution was the goal of new techniques (Gao *et al*. 2006; Hansen *et al*. 2008; Hilker *et al*. 2009, Sedano *et al*. 2014). But then, the solutions were found to be not unique and less well suited to predict sudden (observed) changes (Hilker *et al*. 2009, Sedano *et al*. 2014).

The approaches can be considered as examples of finding solutions of an inverse problem. The inverse problem consists of using the actual result of some measurements to infer values of model parameters and predict values of the parameters that characterize the system (Tarantola 2005), e.g. Landsat temporal changes: synthetic Landsat time series to monitor vegetation dynamics (Hilker *et al*. 2009). In contrast, improving the spatial interpretation of observed trends by estimating their response from a particular subsurface structure is what can be considered the forward problem (Tarantola 2005) or a disaggregation method.

For instance, the Landsat-derived deforestation of Tucker and Townshend approach (2000), or the VHR-derived very high spatial resolution long-term changes in the density of trees and shrubs in the Sahel (Gonzalez *et al*. 2012; Brandt *et al*. 2016) or the harmonized Landsat-Sentinel-2-combined high frequency monitoring time series are all resolved as forward problems. While the forward problem has a (deterministic) unique solution, the inverse problem does not (Tarantola 2005) as the authors of the synthetic Landsat time series approach have found out. In all these approaches, a priori knowledge of the scene is necessary and it has to be made explicit as an input of model parameter: a Kalman-based fusion filter (Sedano *et al*. 2014) or spatial and temporal empirical adaptive filters (Gao *et al*. 2006; Hansen *et al*. 2008; Hilker *et al*. 2009) or a semi-empirical fusion approach using MODIS and BRDF (Roy *et al*. 2008).

However, the harmonization of ESA's Sentinel-2a and Sentinel-2b data with Landsat-8 data could be used as a priori information to improve long-term Landsat synthetic time series but still the synthetic approach won't be suited for sudden changes. In fact, in most cases such recovery cannot be done exactly because the mathematical models are approximations, data are noisy, and the number of observations finite.

Moreover, obtaining a solution may require further approximations for efficient numerical computations that are computationally intensive and prohibitive when extending such approaches to obtain a synthetic VHR time series and even unnecessary. Instead, since we aim to capitalize on the spatial detail provided by VHR commercial data to improve mapping and spatial interpretation of the temporal trends, we can focus on providing spatial detail with VHR spatial variance and thus resolve the characteristics of the trends by their 0.5m elements.

II.2. METHODS: VIEWING DISAGGREGATION AS A FORWARD PROBLEM

Instead of trying to generate a synthetic medium or VHR spatial resolution time series for continuous monitoring, we build upon these results in terms of a forward/inverse problem. By combining high spatial resolution with high temporal resolution data, we aim to capitalize on the spatial detail and the temporal regularity of acquisitions, provide enough spatial detail to identify attribution and separation of the effects of changes and provide a practical operational method to improve interpretation of trends, e.g. the type of degradation or drivers.

The observations we are interested in are of the form,

$$\mathrm{NDVI}_{\_\mathrm{modis}}(x0,y0) = \sum \mathrm{NDVI}_{\_\mathrm{Landsat}}(x,y)\, f(x,y)$$

The integration or sum is over a neighborhood of 250 m around $(x0, y0)$ such that, $\|x0-x\|<125$ and $\|y0-y\|<125$ and $f(x, y)$ is a weighting factor (a density function). The inverse problem is to find $\mathrm{NDVI}_{\_\mathrm{Landsat}}$ in terms of $\mathrm{NDVI}_{\_\mathrm{modis}}$. Given a solution to an inverse problem, we have to identify which of its features are real and which are (noise) artifacts or systematic modeling errors. Instead, we can integrate Landsat data to the resolution of MODIS and find the spatial variability that allows us to reconstruct the actual values of Landsat. From here the methodology for disaggregation, aggregation is straightforward (see steps 1-11 below). Since the availability of Landsat cloud-free data limit the periods of the season where we can do this integration, the comparison of the variability between different years could be within different phenology periods. Thus, we need to find a way to normalize the variability.

The annual integrals of NDVI from MODIS/AVHHR summarize the variability for each year at each $(x0, y0)$. This value per each 250 m pixel provides a way to normalize any Landsat value regardless of the period taken.

In this case, what Landsat provides is the spatial variability of such period, a characterization of elements compositing a pixel at 30 m spatial resolution. That is, the algorithm for disaggregation is:

Step 1: compute mean NDVI value of Landsat at each MODIS cell per a given period: $\mathrm{AVG}_{\mathrm{Landsat}}(x0, y0)$

Step 2: compute residuals: $\mathrm{LandsatR}(x, y) = \mathrm{Landsat}(x, y) - \mathrm{AVG}_{\mathrm{Landsat}}(x0, y0)$, where $\|x0-x\|<125$ and $\|y0-y\|<125$

Step 3: compute $\mathrm{MODIS}(x0, y0)$ annual integral corresponding to the year from where $\mathrm{Landsat}(x, y)$ is available

Step 4: normalize Landsat: $\mathrm{Landsat}_{\mathrm{N}}(x, y) = \mathrm{Landsat}_{\mathrm{R}}(x, y) + \mathrm{MODIS}(x0, y0)$

Step 5: compute histograms for each $\mathrm{Landsat}(x, y)$ and $\mathrm{Landsat}_{\mathrm{N}}(x, y)$ to show seasonal adjustments

Step 6: compute annual integral soil-based MODIS value from the MERRA2 soil moisture, $\mathrm{MODIS}^{t}_{\_\mathrm{Soil}}(x0,y0)$, for climate-adjusted analysis of trends (RESTREND).

Step 7: take any year as baseline for climate, say $\mathrm{MODIS}^{t0}_{\_\mathrm{Soil}}(x0,y0)$.

Step 8: compute residuals of $\mathrm{MODIS}_{\_\mathrm{Soil}}(r(t))(x0,y0) = \mathrm{MODIS}^{t}_{\_\mathrm{Soil}}(x0,y0) - \mathrm{MODIS}^{t0}_{\_\mathrm{Soil}}(x0,y0)$.

Step 9: adjust Landsat to climate effects, $\mathrm{Landsat}_{\mathrm{NClim}}(x, y) = \mathrm{Landsat}_{\mathrm{N}}(x, y) + \mathrm{MODIS}_{\_\mathrm{Soil}}(r(t))(x0,y0)$

Step 10: compute histograms for each $\mathrm{Landsat}_{\mathrm{NClim}}(x, y)$.

Step 11: Merge VHR data and $\mathrm{Landsat}_{\mathrm{NClim}}(x, y)$ at the 50 cm VHR resolution by repeating $\mathrm{Landsat}_{\mathrm{NClim}}$ values as necessary.

II.3. RESULTS

To evaluate the results of incorporating higher-resolution data for disaggregation or targeted analysis, pilot sites have been selected. We selected these sites based on 73 CI-Vital Signs (CI-VS) select priority sites with known types of degradation and 21 regions reported having negative trends in our previous report (Tucker and Pinzon 2017). Figure B1 show the regions of interest with negative trends in Kenya, Uganda and Senegal and also the CI-VS select sites in Tanzania where VS has developed and implemented an integrated set of protocols for filed-based monitoring of degradation and vegetation productivity (http://vitalsigns.org/sampling-frame).

We focus on this report on the 21 regions to evaluate the landscape characteristics of the regions with negative trends without field measurements. The areas chosen for disaggregation allow us to test the contribution of incorporating VHR imagery and medium resolution Landsat imagery for interpretation. From these sites, we show results for 4 regions covering 7 sub-tiles. These examples are used to clarify and illustrate the type of applications of the methods proposed for the toolbox CI-VS is developing to support monitoring of land degradation. In the coming report, we evaluate this integration and disaggregation when field measurements and specific knowledge of type of degradation is available. These examples are simplifications that capture the essence of more complex questions that could arise in applications where interpretation of trends would require much more background and even more precise ground data to explain fully. Similar analysis (not shown) was performed over the remaining 14 sub-tiles (Figure B1).

Figure 4 shows a panchromatic VHR-sub-tile around region RA (Figure B1 around Kampala, Uganda) before contrast correction (ranging from -10 to 1600), after contrast correction VHRcc (ranging from -350 and 350) and corresponding normalized $Landsat_{NClim}$ imagery (steps 1-10) with added VHRcc spatial variability for 1995 and 2016 (step 11). Notice that the added VHRcc spatial variance does not affect the original Landsat spatial patterns since the coherence of Landsat NDVI at 30 m still dominates spatial features and variability. The histogram of VHRcc (Figure 4c) is almost (Gaussian) with zero mean value. Also noticeable is the bump around -100 that captures the spatial variability around light cloud-shadows (shadows in top-right Figure 4B) that biased the histogram towards the bump.

Figure 5 shows normalized $Landsat_{NClim}$ for years 1995, 2010 and 2015, all with the same enhancing VHRcc spatial variability and the corresponding Landsat histograms before (Figure 5B) and after climate correction (Figure 5C) using the AVHRR/MODIS NDVI annual integrals corresponding to the region (Figure 5A). Notice the shifting of the histograms of the 2015 image towards the right, after climate correction is performed. In fact, the NDVI capture the double seasonality in the region and it tends to be lowest at the end of February (see time series in Figure B3) implying that the normalization attenuates the effects of phenology and allows fair comparisons, a feature of interest when defining baselines. The normalization of Landsat imagery is intended to attenuate seasonal effects and climate effects (Step 1-10 in methodology). The marked regions of interest (R1, R2, R3, and R4) are selected for further study (Figures 9-12).

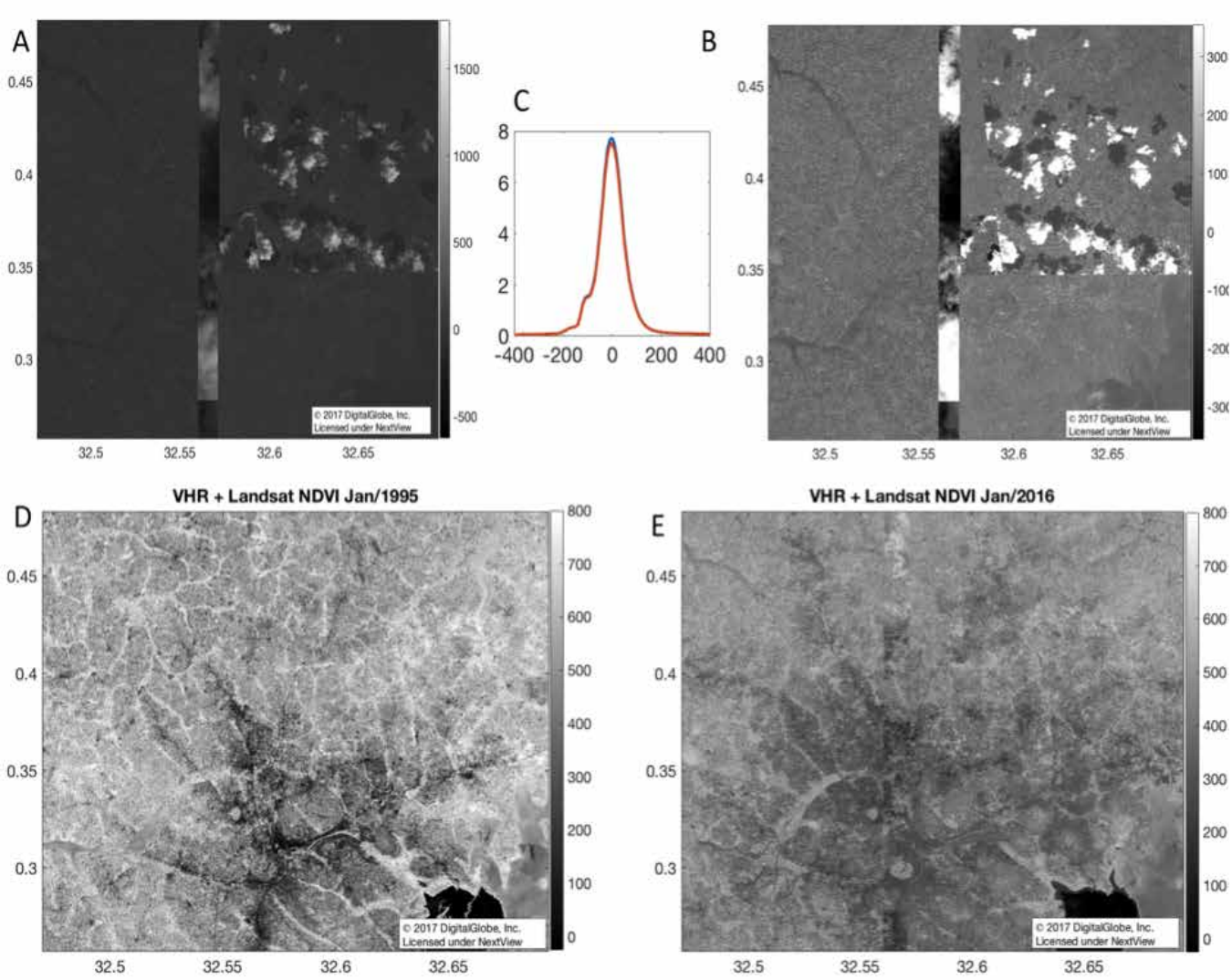

Figure 4. Panchromatic commercial VHR mosaic sub-tile (A) before contrast correction, B) after contrast correction subtracting the mean (VHRcc = VHR – mean(VHR)); very reflective clouds (VHRcc>350) and their darker shadows (VHRcc<-350) are flagged out as 410 and -410 respectively. C) The histogram of the resulting VHRcc image where clouds and shadows are not filtered out. Fusion of the VHRcc with D) the normalized $Landsat_{NClim}$ for 1995, and E) the normalized $Landsat_{NClim}$ for 2016 at the resolution of VHRcc. For zooms of the fusion see Figures 9 and 10.

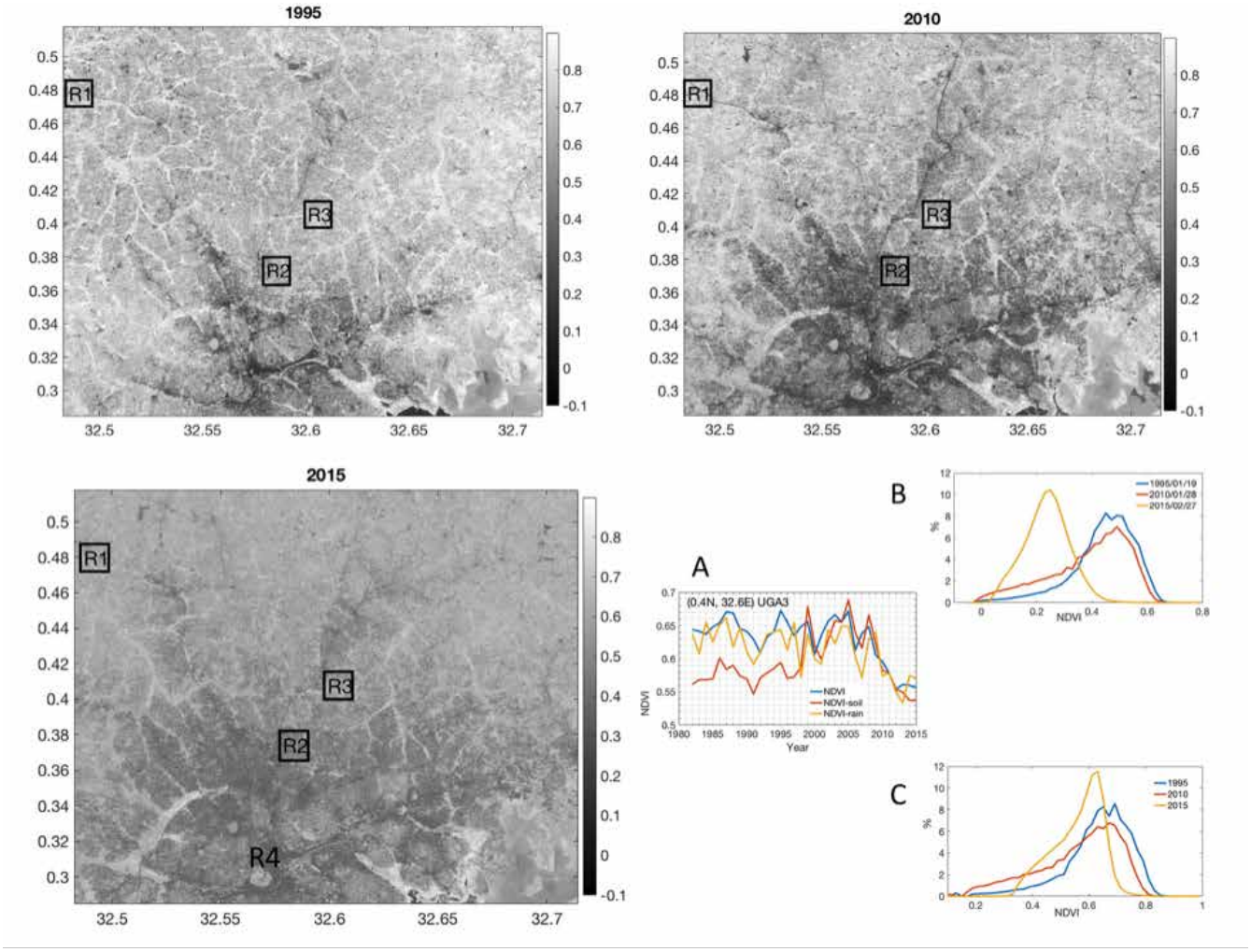

Figure 5. Adjustment of Landsat from different years (1995, 2010, 2015) using the A) AVHRR and MODIS soil-adjusted NDVI integral annual value (NDVI-soil from MERRA2) corresponding to each year (step 1-10 methodology); regions of interest (R1, R2, R3) for further study are marked on each image. The histograms computed from B) the original Landsat imagery and from C) the normalized Landsat images.

Figure 6, 7 and 8 show similar results of the Landsat annual climate normalization and spatial enhancement with corresponding VHRcc sub-tiles for regions RB, RC, and RD (Figure B1). In Figure 6, all histograms but 2000's converge to a similar peak; the 2000 image was affected by missing values on the left side of the image (dark areas) over most of the pixels which dynamic range of variation should be between 0.2-0.9, thus the 2000 image is not representative of the region (too many missing values).

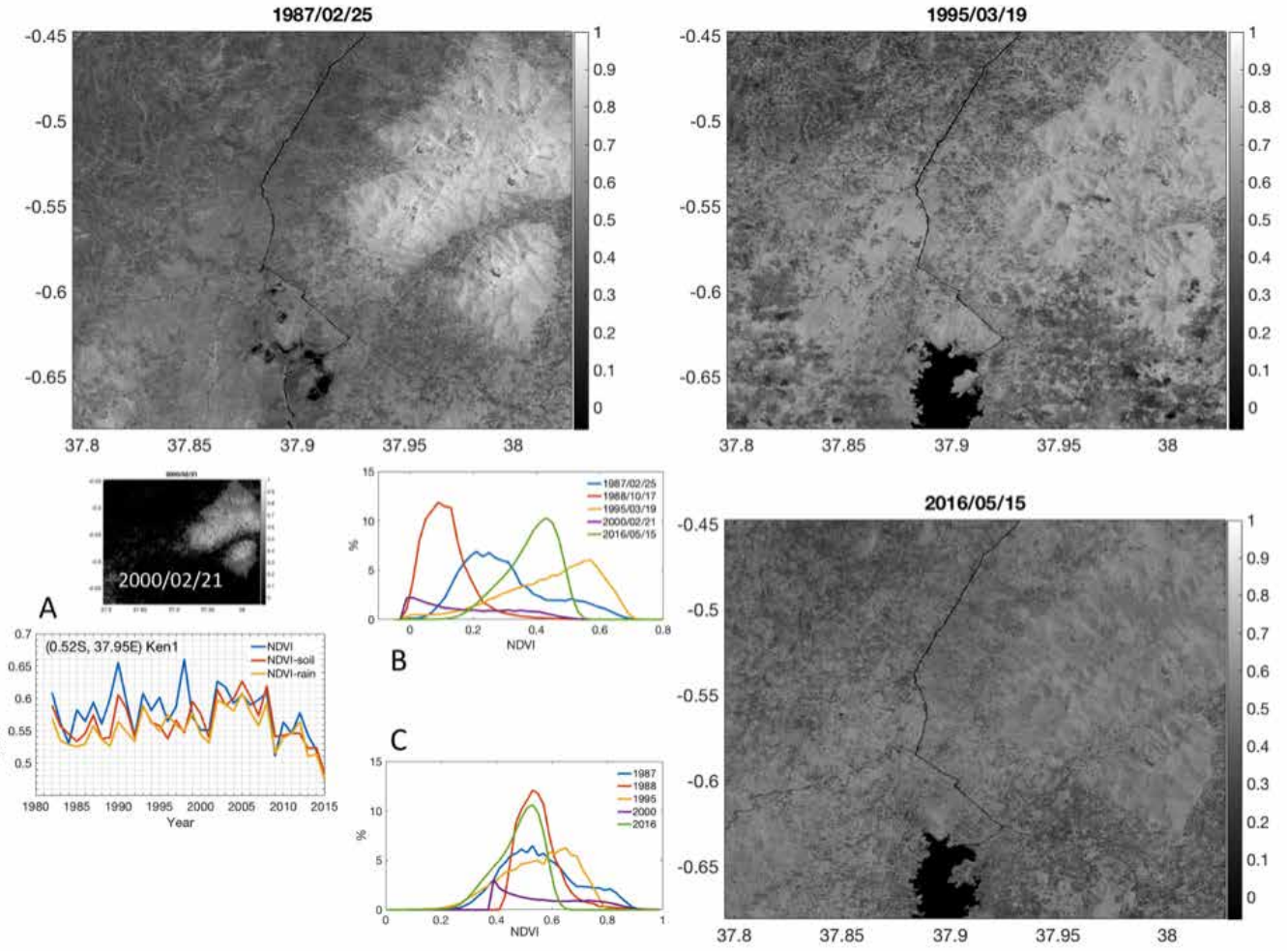

Figure 6. Adjustment of Landsat from different years (1987, 1988 (not shown), 1995, 2000, and 2015) using A) AVHRR&MODIS soil-adjusted NDVI integral annual value (NDVI-soil) that correspond to each year (step 1-10 methodology). The histograms computed from B) the original Landsat imagery and from C) the normalized Landsat images.

The normalization of Landsat imagery is intended to attenuate seasonal effects and climate effects (Step 1-10 in methodology). In Figure 6 and 7 (regions RB, and RC), the differences in the histogram shapes suggest the strong seasonal variability within the region. The original (non-normalized) imagery makes the seasonal variations explicit. Still the normalization attenuates these effects. Regions RB, and RC are around Mount Kenya where Global Environment Facility (GEF) initiated a pilot project of best practices for natural resource management and invested in the creation and maintenance of Protected Areas (PAs) from 2007 to 2012.

The convergence in histograms of the normalized Landsat images suggests that the negative trend observed is climate-driven thus the sudden drop of the integrals around 2009 (A). The shape differences in both histograms (original and normalized) suggest a strong seasonal variability within the region. In fact, the NDVI of Mount Kenya captures the double seasonality in the precipitation. The histograms of the normalized LandsatNClim reflect spatial variability in the phenology profiles, but the normalization also shows that all years behave similarly after climate effects are attenuated. The spread of the histograms of the original (non-normalized) imagery makes the seasonal variations explicit.

In Figure 8 (region RD), the homogeneity in the histogram shapes suggests the strong spatial coherence during the dry season within the region. When adjusted for climate effects the negative trends are not significant. The Landsat image for 2016 was taken a month earlier than the others, basically a month before senescence. The normalization attenuates the effects of phenology to make a fair comparison between years. This study corroborates the findings of Gonzalez *et al*. (2012), namely, the negative trends observed are climate-based.

However, without a corresponding VHR images from the 1980s-1990s or early 2000s, our interpretation of normalized histograms is limited. Gonzalez *et al*. (2012) uses Ikonos satellite images and historical aerial photographs to determine current and past tree densities that they corroborated with field measurements of trees (see Figure B2 for a DigitalGlobe VHR image showing current tree distribution).

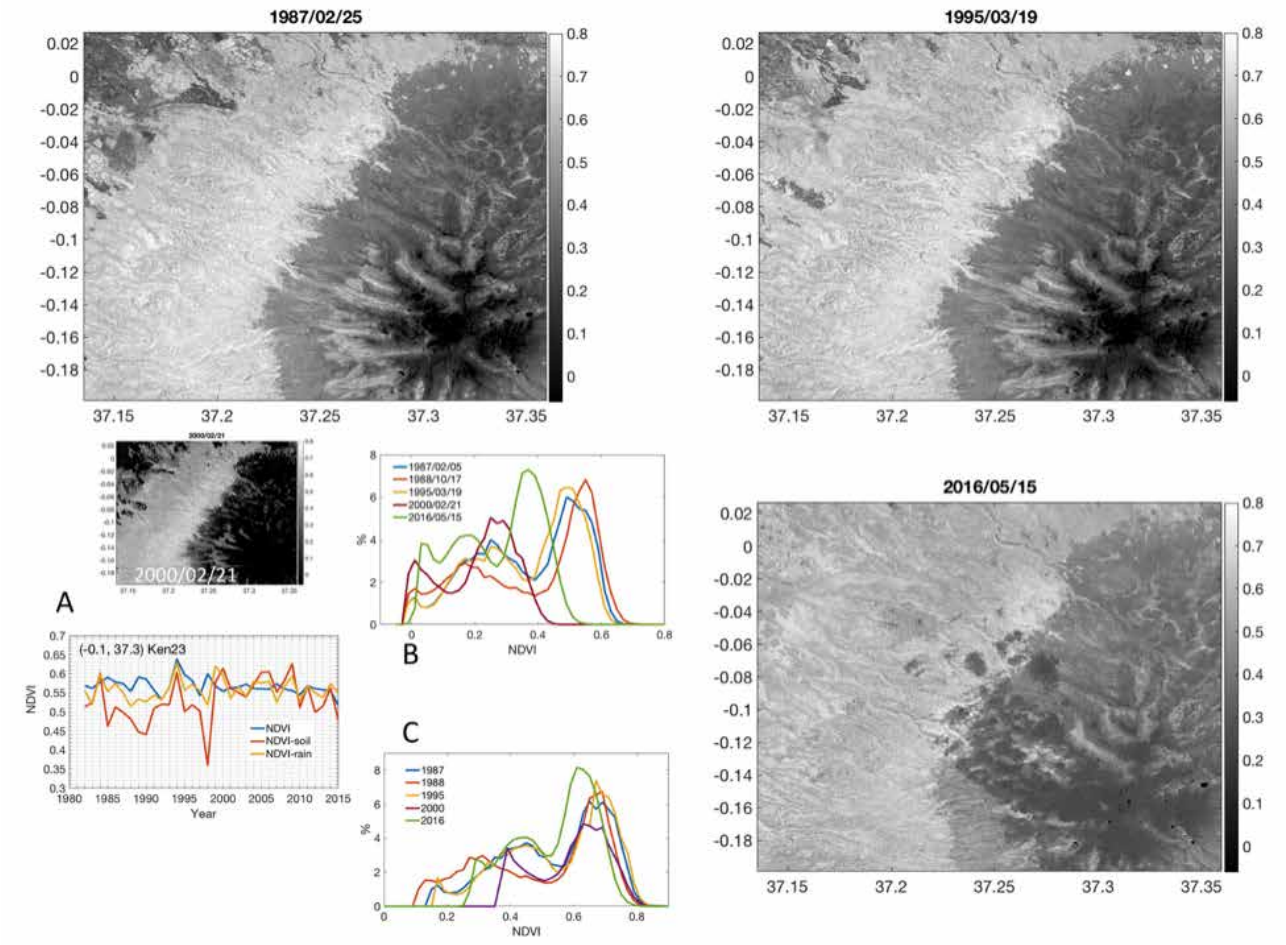

Figure 7. Adjustment of Landsat from different years (1987, 1988 (not shown), 1995, 2000, and 2015) using the A) AVHRR and MODIS soil-adjusted NDVI integral annual value (NDVI-soil) corresponding to each year (step 2 methodology). The histograms computed from B) the original Landsat imagery and from C) the normalized Landsat images. All histograms converge to a similar peak, even 2000 that were affected by clouds on the right side over pixels with adjusted NDVI values between 0.2-0.4 (notice the drop in the 2000 histogram below the 0.4 NDVI mark). The normalization of Landsat imagery is intended to attenuate seasonal effects and climate effects (Step 2 in methodology). Again the convergence in C) suggests no land degradation since the drops in NDVIs after 2011 are climate-driven.

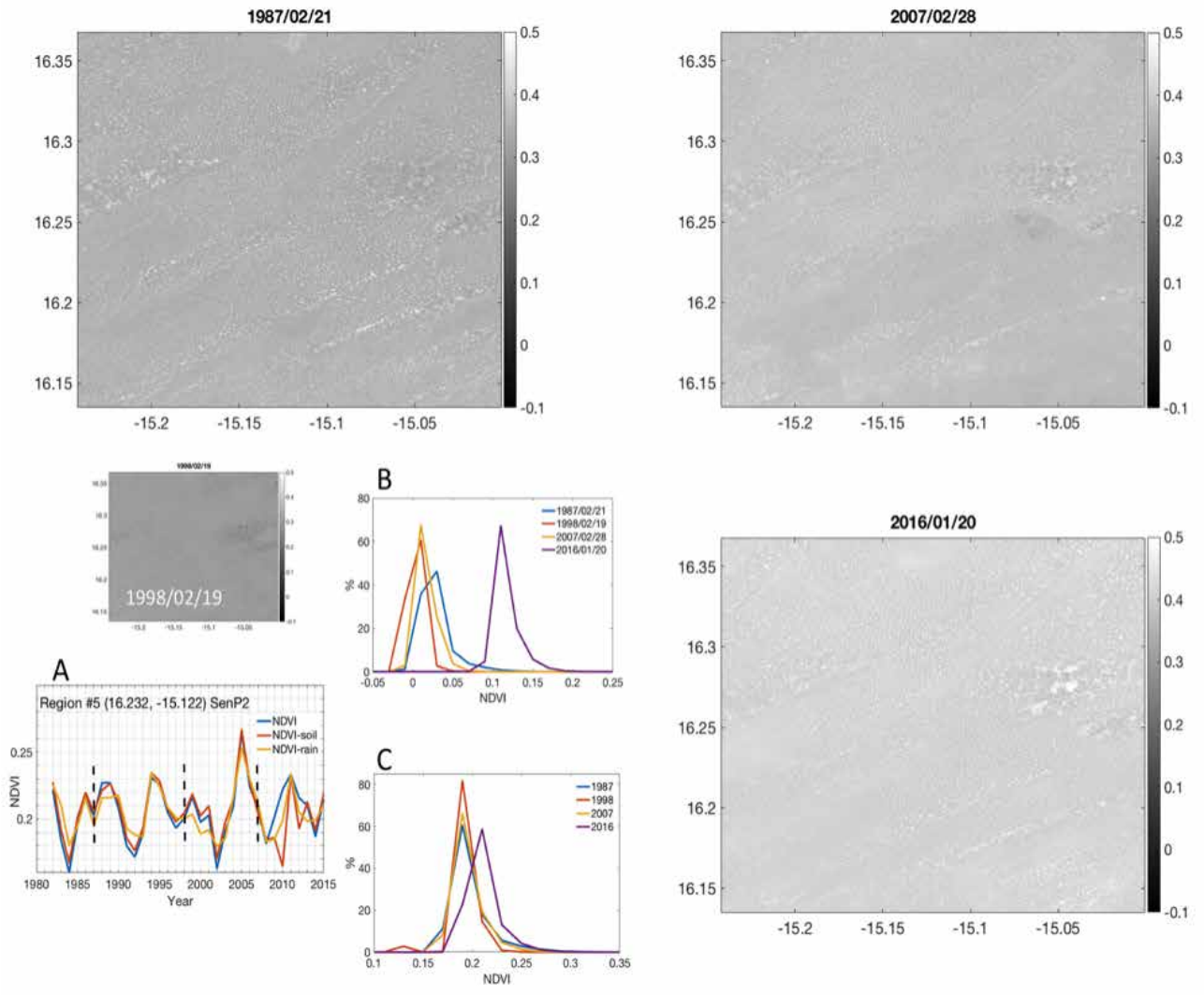

Figure 8. Adjustment of Landsat from different years (1987, 1998, 2007, and 2016) using the A) AVHRR and MODIS soil-adjusted NDVI integral annual value (NDVI-soil) corresponding to each year (steps 1-10 methodology); region of interest RD in Figure B1. The histograms computed from B) the original Landsat imagery and from C) the normalized Landsat images. Notice the shifting in all histograms when the (B) original Landsat images are (B) adjusted for climate contribution.

II.4. DISCUSSION

Figure 9 and 10 show 1 km zooms of normalized 1995 and 2016 NDVI VHR+LandsatclimN for regions R1, R2, R3, and R4 around Kampala, Uganda (see Figure 5 for locations). Two features come to light: a) Landcover: region R1 is mostly forest and crop-fields in both years, region R2 and R4 are urban areas and region R3 is being transformed from forest (1995) to urban development (2016).

R3 was identified as degraded in our previous report output1.1.1. b) Spatial coherence: the elements of VHR within LandsatclimN are more congruent in 2016 than 1995 since VHR images in the mosaic come from 2011-2015. This difference is more clear in regions R3 and R4 where the (spatial) elements of VHR highlights the changes in development during the two years, e.g. the evolution of the round plaza in region R4. Congruence would be a feature to consider when interpreting changes in landcover.

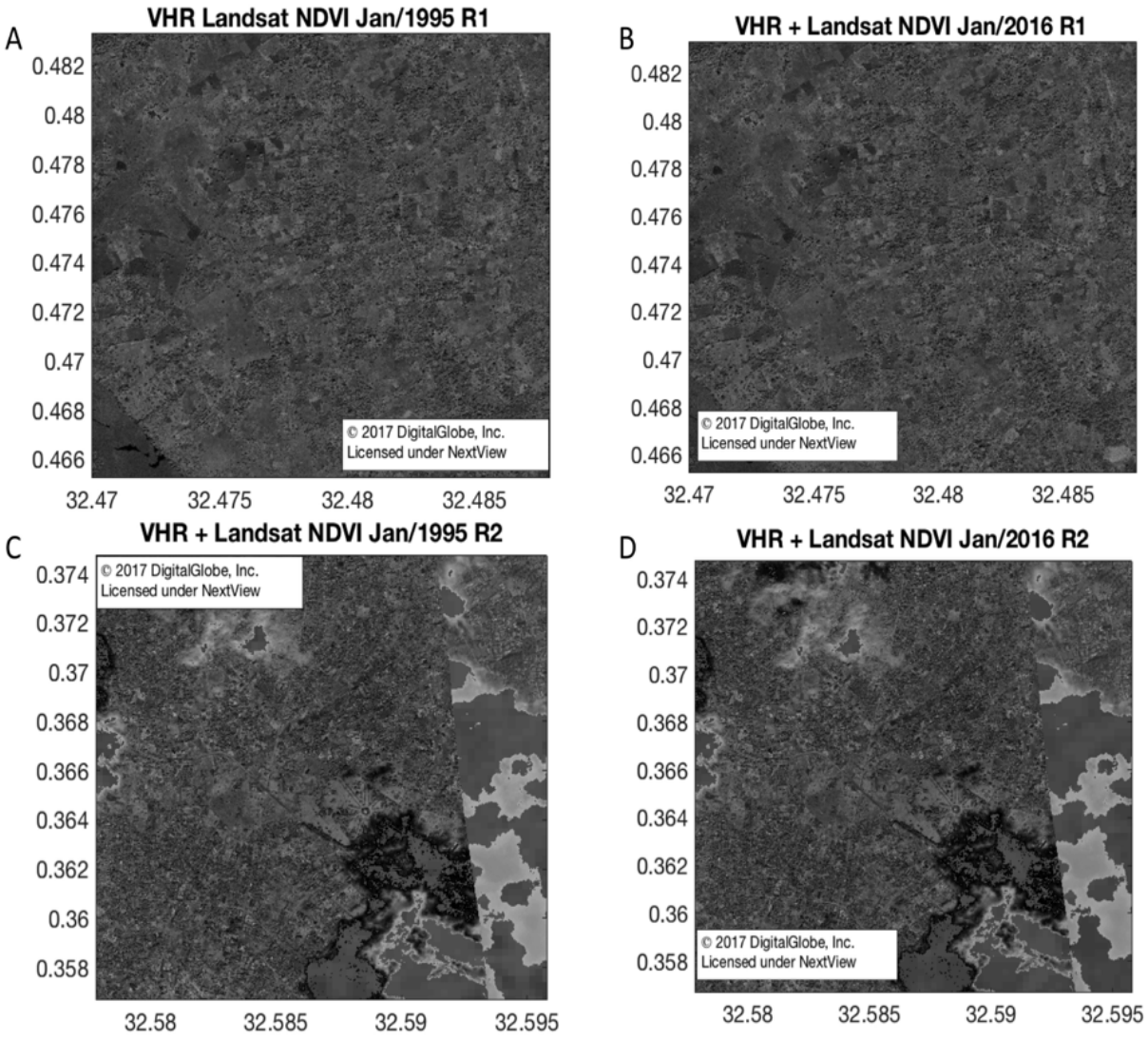

Figure 9. Zooming of region R1 for A) 1995 and B) 2016 and region R2 for the same years C) 1995 and D) 2016 of the fusion of adjusted VHRcc panchromatic and corresponding Landsat images (Figure 4B). From Figure 4, VHRcc suffers from cloud-cover issues around R2 region – the Landsat 30 m value then filled the gaps. The cloud-cover regions where the correspondent Landsat year fills the gaps show very similar spatial (Landsat) patterns but still with small spatial differences, indicating that the variance contributions are similar at each year in both regions. The differences are a little more noticeable in region R2. This is consistent with the histograms by region and years in Figure 11.

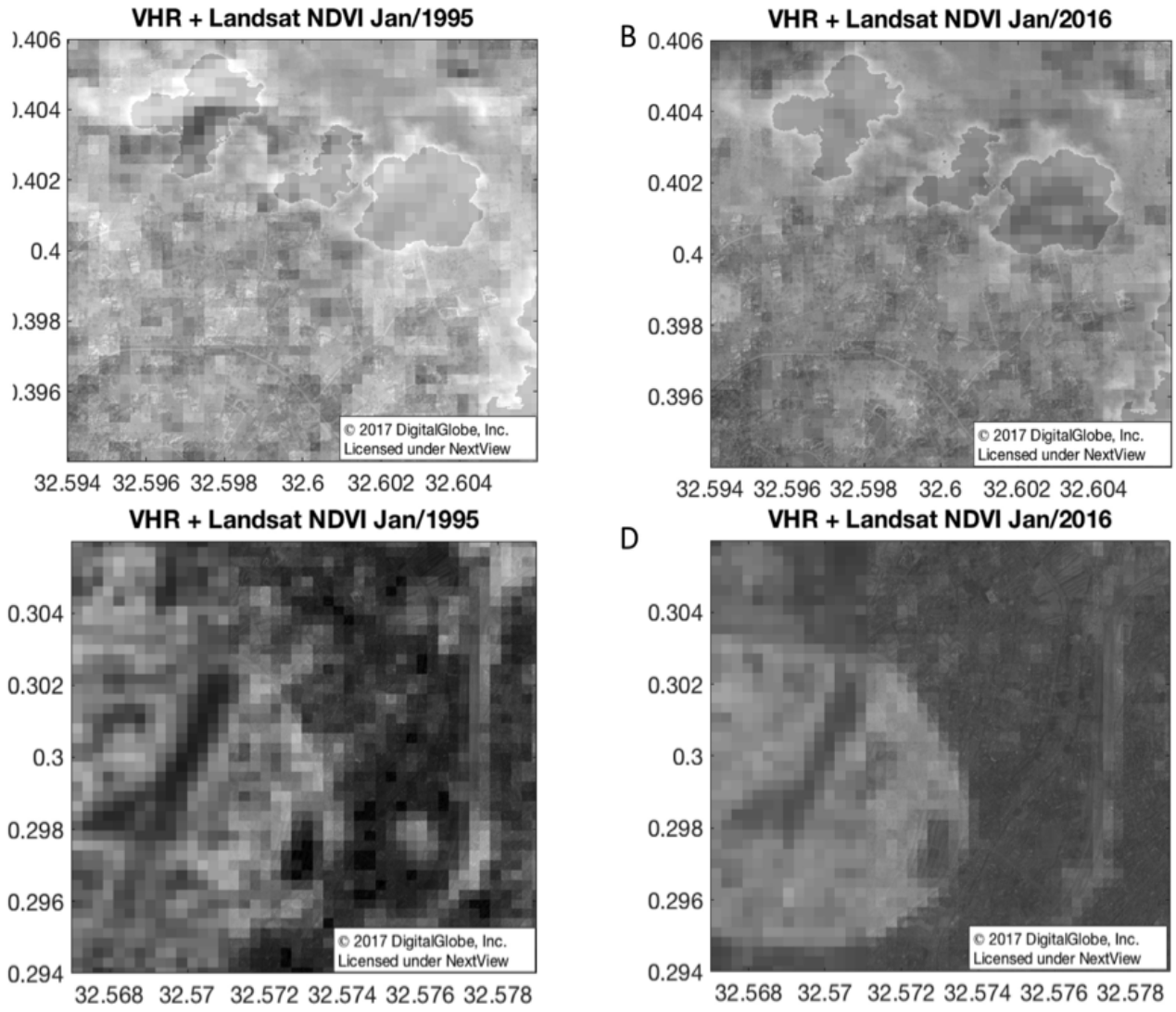

Figure 10. Zooming of region R3 for A) 1995 and B) 2016 and region R4 (See Figure 5 for location) for the same years C) 1995 and D) 2016 of the fusion of adjusted VHRcc panchromatic and corresponding Landsat images (Figure 4B). From Figure 4, VHRcc suffers from cloud-cover issues around R3 region. The spatial variance in these regions allows us to study potential spatial harmony as confirmation of consistency of elements. The normalized NDVI-Landsat from 1995 is higher than the corresponding NDVI for 2016. However, we can see that there is more homogeneity in the 2016 images, suggesting that the year of the image making the mosaic in VHRcc is closer to 2016 (Pinzon *et al*. 2001). In fact, Figure B3 shows the exact dates of the images making the mosaic in this sub-tile. The images came from 12/1/2013 for R3 and 12/20/2013 for region 4. The fusion occurs smoothly when the images being merged are coherent – they corroborate with each other (Pinzon *et al*. 2001). The congruence of the circular plaza in R4 is remarkable. On the other hand, the incongruity suggests that there are changes on the region between the years merged that are worth investigation.

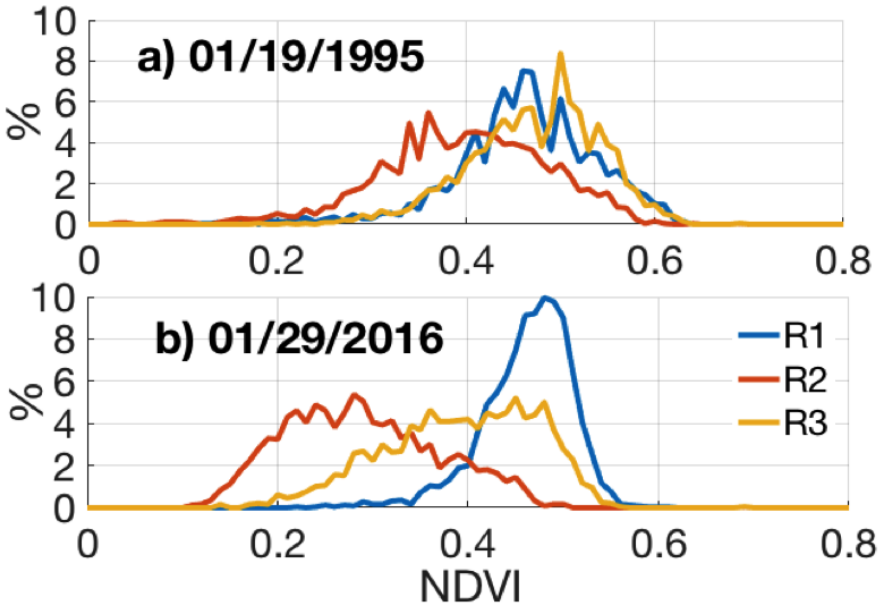

Figure 11. Histogram of normalized climate-adjusted histograms for 1 km subsets around regions R1, R2, and R3 (see Figure 5) during 1995 and 2016. The histograms capture the spatial variability at 30 m resolution on a) January 19 of 1995 or b) January 29 of 2016.

Figure 11 shows details of the histogram of normalized LandsatclimN NDVI 1km subsets for regions R1, R2 and R3 (see Figure 5). It also highlights the changes occurring in the regions, e.g region R3 from forest to urban development. The 1995 histograms for regions R1 and R3 show similarities of the forest landcover. Region R2 is characterized by urban developments. The shifting of the histograms is also corroborated by the decadal climatology contrasted in Figure B3. The difference between the histograms of 1995 and 2016 for region R1 could reflect either a ten-day difference in the seasonality or a more controlled or homogeneous land management in 2016. To dispel the difference, we would need more knowledge of the regions via historical field measurements.

Figure 12 show patterns of NDVI from 0.5 m VHR NDVI-pan-sharpen mosaics and NDVI from recent 30 m Landsat imagery that correspond to the same regions in Figure 5 around Kampala, Uganda (Kampala). Similar spatial patters are observed at this spatial extent, although, cut-lines and cloud-cover regions (very dark spots) are evident in the VHR mosaic. Figure 12 also show corresponding zooms for region R3, where recent building infrastructure (development expansion) is occurring: 0.5 m VHR NDVI-pan-sharpen zoom (12/01/2013, see Figure B4 for dates of acquisition) and 0.5 m Landsat NDVI-VHR sharpen zoom (Jan/2016).

Notice the harmony of the January spatial features of the combined Landsat-VHR fusion despite of being 3 years apart (2013 and 2016). We argue that because of this harmony, the Landsat-VHR fusion provides more useful information for interpretation than the 0.5 m VHR NDVI-pan-sharpen, we can even see useful NDVI features through the clouds although at (squared) 30 m resolution. This opens new possibilities not only for speeding up the mosaic processing by prioritizing panchromatic mosaic processing only and combining them with the Landsat archive.

Potentially the VHR panchromatic processing could be extended to some periods of the year, e.g.x` by seasons (Jan-Mar, Apr-Jun, Jul-Sep, and Oct-Dec) for every three-five years or by year if available. Since processing of the panchromatic VHR images normalizes each image that are part of the mosaic to improve spatial contrasts and thus, improves element discrimination, the merging of 30 m NDVI-Landsat will provide the temporal information of a time series.

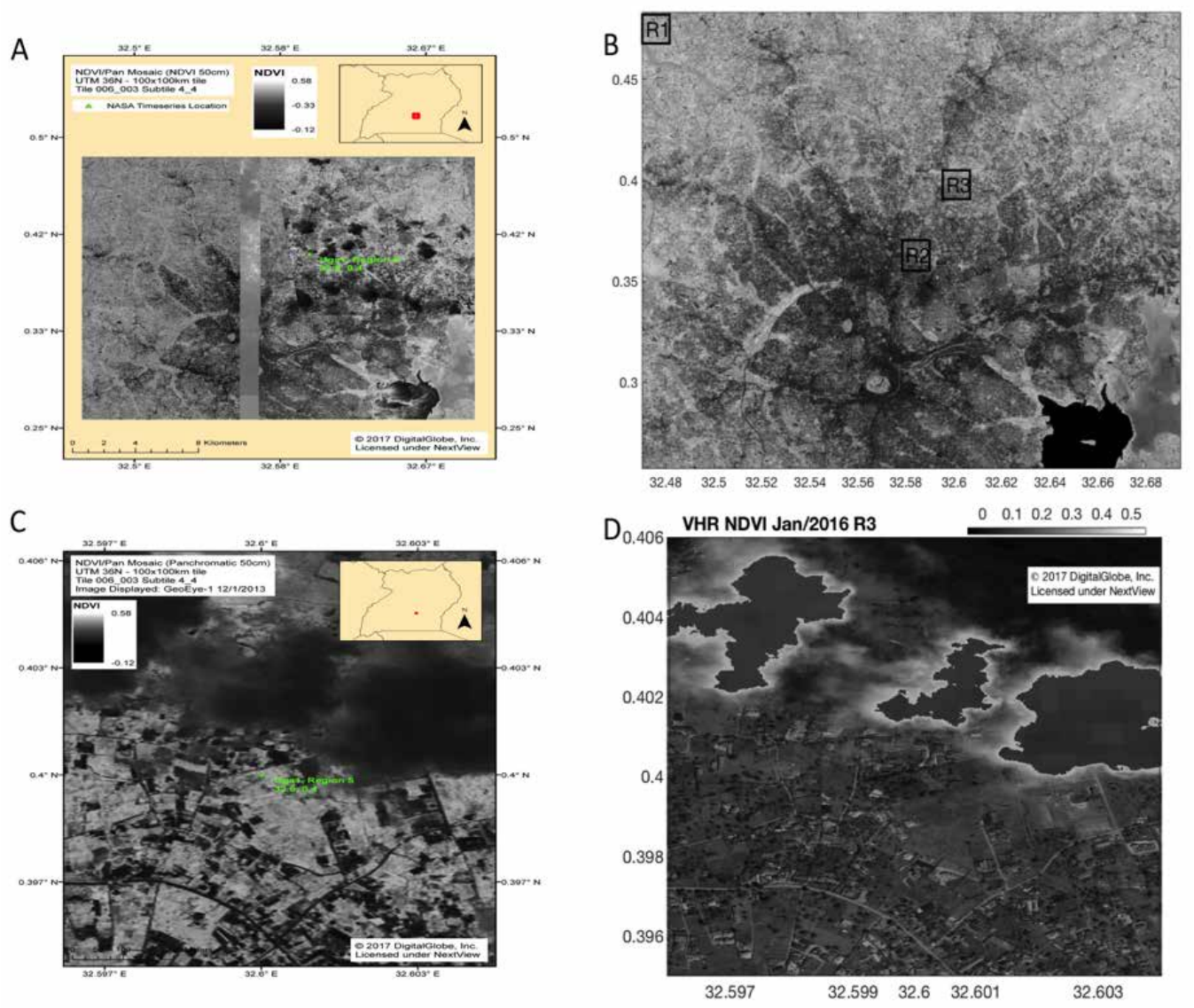

Figure 12. Patterns of a) NDVI from 0.5m VHR NDVI-pan-sharpen mosaics and b) NDVI from recent 30m Landsat imagery that correspond to selected ROI in Figures 5, within near the capital, Kampala, Uganda (Kampala). Similar spatial patters are observed at this spatial extent, although, cut-lines and cloud-cover regions (very dark spots) are evident in the VHR mosaic. Corresponding zooms for region R3, where recent building infrastructure (development expansion) is occurring, c) 0.5m VHR NDVI-pan-sharpen zoom (12/01/2013, see Figure B4 for dates of acquisition) and d) 0.5m Landsat NDVI-VHR sharpen zoom (Jan/2016).

II.5. CONCLUSIONS

The availability of high temporal but coarse spatial resolution (from 1982 (AVHRR), 2000 (MODIS)), medium spatial resolution (from Landsat 1982 (TM, ETM+, OLI) harmonized with Sentinel-2 (2015)) and high spatial resolution (from 2002) data offers an unprecedented possibility to exploit their synergy to greatly expand the multi-temporal change detection from coarse spatial resolution to a multi-scale analysis and improve interpretations of trends. In this study, we aim to capitalize on the spatial detail and the temporal regularity of acquisitions and provide enough spatial detail to identify attribution and separation of the effects of changes and thus improve mapping and interpretation of trends, e.g. the kind of degradation or drivers.

We chose case studies to clarify and illustrate the type of applications of the methods proposed for the toolbox. These examples are simplifications that capture the essence of more complex questions that could arise in applications where interpretations of trends would require much more background and even more precise ground data to explain fully.

There was high harmony between AVHRR/MODIS, Landsat and panchromatic VHR imagery. We argue that because of this harmony, the Landsat-VHR fusion provides useful information for interpretation than the 0.5m VHR NDVI-pan-sharpen, e.g., NDVI features through the clouds although at (squared) 30m resolution.

This opens new possibilities not only for speeding up the mosaic processing by prioritizing panchromatic mosaic processing only and combining them with the Landsat archive but also to exploit the most frequent harmonized" reflectance products from combined Landsat, Sentinel-2a, and Sentinel-2b observations. Potentially the VHR panchromatic processing could be extended to some periods of the year, say by seasons (Jan-Mar, Apr-Jun, Jul-Sep, and Oct-Dec) for every three-five years or by year if available. Since processing of the panchromatic VHR normalizes each image composing the mosaic to improve spatial congruent contrasts and thus, improves element discrimination, the merging of 30m NDVI-Landsat will provide the temporal information of a time series that we don't have with only NDVI VHR processing.

Kanuku Mountains, South America. © Pete Oxford/ iLCP

III. CONCLUSIONS AND GUIDANCE

We have detailed a simple 11-steps pan-sharpen approach that combines the temporal regularity of AVHRR (8000m), and MODIS(250m) imagery with higher spatial resolution Landsat (30m) and VHR (0.5m) commercial data to provide spatial detail and context for disaggregation of temporal trends for better interpretation (see section II.2). Moreover, we have identified the limitations of producing a VHR mosaic from more than 188000 images.

We recommend extending the VHR panchromatic processing to more periods during the year, say by seasons (Jan-Mar, Apr-Jun, Jul-Sep, and Oct-Dec) and for epochs of every three-five years or by year if available. Still the spatial detail gained from one mosaic has allowed us to interpret components of a region as drivers of the observed trends.

This interpretation would be much more detailed if more epochs and seasons of the VHR are available. We have applied a simple Pan-sharpen technique to add spatial detail that allows us to interpret observed trends. The simplicity of the approach would facilitate their inclusion and implementation in the toolbox.

However, to analyze and interpret these time series more profoundly, takes much more experience and theoretical understanding than what can be conveyed during a short training course. If we were to take another step in the analysis – by introducing the kind of techniques described in this report (1.1.2) – we would need some changes to the project: 1) involving (only) specialist on remote sensing and 2) invest much more in capacity building. We have also followed the updated guidelines on NextView Licensed imagery by using VHR JPEG geo-reference images to disaggregate elements from coarser resolutions and adding copyright burned into our results.

Tea plantations in eastern Rwanda. © Levi S. Norton

IV. REFERENCES

IV. REFERENCES

Albalawi, E. K. and Kumar, L. (2013). Using remote sensing technology to detect, model and map desertification: A review. Journal of Food, Agriculture and Environment, 11, 791-797.

Anyamba, A. and Tucker, C. J. (2012). Historical perspective of AVHRR NDVI and vegetation drought monitoring. Remote Sensing of Drought: Innovative Monitoring Approaches, 23.

Brandt, M. *et al.* (2016). Woody plant cover estimation in drylands from Earth observation based seasonal metrics. Remote Sensing of Environment 172:28-38.

Carper, W. J., Lillesand, T. M., and Kiefer, R. W. (1990). The use of intensity–hue-saturation transformations for merging SPOT panchromatic and multispectral image data. Photogrammetric Engineering and Remote Sensing, 56, 459–467.

Cohen, W. B., & Goward, S. M. (2004). Landsat's role in ecological applications of remote sensing. Bioscience, 54, 535–545.

Coops, N. C., Johnson, M., Wulder, M. A., and White, J. C. (2006). Assessment of QuickBird high spatial resolution imagery to detect red attack damage due to mountain pine beetle infestation. Remote Sensing of Environment, 103, 67–80.

de Jong, R., *et al.* 2011. Quantitative mapping of global land degradation using Earth observations. International Journal of Remote Sensing, 32(21), 6823-6853.

Fensholt, R., Langanke, T., Rasmussen, K., Reenberg, A., Prince, S. D., Tucker, C. J., *et al.* (2012). Greenness in semi-arid areas across the globe 1981–2007 — An earth observing satellite based analysis of trends and drivers. Remote Sensing of Environment, 121, 144–158.

Gao, F., Masek, J., Schwaller, M., and Hall, H. (2006). On the blending of the Landsat and MODIS surface reflectance: Predicting daily Landsat surface reflectance. IEEE Transactions on Geosciences and Remote Sensing, 44, 2207–2218.

Gonzalez, P., Tucker, C. J., and Sy, H. (2012). Tree density and species decline in the African Sahel attributable to climate. Journal of Arid Environments, 78, 55–64.

Hansen, M. C., Roy, D. P., Lindquist, E., *et al*. (2008). A method for integrating MODIS and Landsat data for systematic monitoring of forest cover and change in the Congo Basin. Remote Sensing of Environment, 112, 2495–2513.

Hilker, T. *et al.* 2009. Generation of dense time series synthetic Landsat data through data blending with MODIS using a spatial and temporal adaptive reflectance fusion model. Remote Sensing of Environment 113:1988-1999.

Mandanici, E. and Bitelli, G. (2016). Preliminary comparison of Sentinel-2 and Landsat-8 Imagery for a combined use. Remote Sensing 8:1014-1024.

Markham, B.L., Storey, J. C., Williams, D. L., and Irons, J. R. (2004). Landsat sensor performance: History and current status. IEEE Transactions on Geoscience and Remote Sensing, 42, 2691–2694.

Masek, J. *et al.* (2016). Harmonizing Landsat and Sentinel-2 reflectances for better land monitoring. NASA GSFC Hydrospheric and Biospheric Science. http://hls.gsfc.nasa.gov/ and https://nex.nasa.gov/nex/projects/1371 accessed on January 20, 2017.

Pinzon, J.E., Pierce, J.F., Tucker, C.J., and Brown, M.E. (2001). Evaluating Coherence of Natural Images by Smoothness Membership in Besov Spaces, IEEE Trans. on Geoscience and Remote Sensing, Vol. 39 (9): 1879-1889

Pohl, C., van Genderen, J.L. (1998). Multisensor image fusion in remote sensing: concepts, methods and applications. International Journal of Remote Sensing, 19(5), 823-854.

Rishmawi, M., Prince, S. D., Xue, Y. (2016). Vegetation responses to climate variability in the northern arid to sub-humid zones of Sub-Saharan Africa. Remote Sensing 8, 910; doi:10.3390/rs8110910.

Roy, P., Junchang, J., Lewis, P., Schaaf, C., Gao, F., Hansen, M., and Lindquist, E. (2008). Multi-temporal MODIS–Landsat data fusion for relative radiometric normalization, gap filling, and prediction of Landsat data. Remote Sensing of Environment, 112, 3112–3130.

Sedano, F., Kempeneers, P., and Hurtt, G. (2014). A Kalman filter-based method to generate continuous time series of medium-resolution NDVI images. Remote Sensing, 6, 12381–12408. doi:10.3390/rs61212381.

Shalaby, A. and Tateishi, R. (2007). Remote sensing and GIS for mapping and monitoring land cover and land-use changes in the Northwestern coastal zone of Egypt. Applied Geography, 27(1), 28-41.

Symeonakis, E. and Drake, N. (2004). Monitoring desertification and land degradation over sub- Saharan Africa. International Journal of Remote Sensing, 25(3), 573-592.

Tarantola, A. (2005) Inverse problem theory and methods for model parameter estimation. SIAM, Philadelphia.

Townshend, J. R., *et al.* (2012). Global characterization and monitoring of forest cover using Landsat data: opportunities and challenges. International Journal of Digital Earth, 5(5), 373-397.

Tucker, C. J., Pinzon, J. E. (2017). Using spectral vegetation indices to measure gross primary productivity as indicator of land degradation, GEF-Land degradation monitoring project, report one: output1.1.1, 1-70. http://vitalsigns.org/gef-ldmp.

Tucker, C. J., Townshend, J. R. G. (2000). Strategies for monitoring tropical deforestation using satellite data. International Journal of Remote Sensing, 21, 1461–1471.

Woodcock, C.E.; Allen, R.; Anderson, M.; Belward, A. *et al.* (2008) Free access to Landsat imagery. Science 2008, 320, doi:10.1126/science.320.5879.1011a.

Wulder, M. A., White, J. C., Goward, S. N., Masek, J. G., Irons, *et al.* (2008). Landsat continuity: Issues and opportunities for land cover monitoring. Remote Sensing of Environment, 112, 955–969.

Yavali, D. D., Tucker, C. J., and Melocik, K. A. (2015). Change in the glacier extent in Turkey during the Landsat Era. Remote Sensing of Environment, 163, 32–41.

Yocky, D. A. (1996). Multiresolution wavelet decomposition image merger of Landsat Thematic Mapper and SPOT panchromatic data. Photogrammetric Engineering & Remote Sensing, 62, 1067–1074.

APPENDIX A. COMMERCIAL HIGH RESOLUTION MOSAICS PROCESSING

The commercial high-resolution mosaic code was originally created by the University of Minnesota's Polar Geospatial Center (PGC) and recently improved at NASA/GSFC. The code corrects for terrain and radiometry, mosaics several images into one set of tiles, and pan-sharpens multispectral images with its panchromatic partner. Two separate mosaic codes are currently in use, one for panchromatic data only and one for NDVI/ PAN data. Mosaics are divided into 100km x 100km tiles and each tile contains 25km x 25km sub-tiles. Mosaic tiles are with a WGS84/ UTM zone specific projection. Due to differences in satellite resolution, all mosaics are resampled to 50cm. For efficient runs, the mosaic code only included imagery with basic levels of image processing from DigitialGlobe, i.e. multispectral product codes M1BS and M4AM as well as panchromatic product codes P1BS and P4AM.

The mosaic codes are run on the NASA Center for Climate Simulation (NCCS) Advanced Data Analytics Platform (ADAPT) which includes a high-performance storage cloud surrounded by large-scale computer resources. We are allocated a number of virtual machine environments (VMs) on NCCS ADAPT (currently 30 VMs each with 4 processors). The number of VMs have varied over the course of the project due to maintenance and shared use from other projects.

Mosaics require multiple processing steps before being created. A general overview of the mosaic processing is shown below.

First, mosaic's extents are derived based on the extents of the project. Once the extents are decided, digital elevation models (DEM) are collected and mosaicked to later be used to ortho-rectify mosaic images. Shuttle Radar Topography Mission (SRTM) digital elevation model (DEM) tiles at 90 meters (version 4) were used for this project. Second, data extents are used to create the tile schema which define the location of each 100km tile (see Figure 3). Tiles are created based on UTM longitude zones and will total 267 tiles over the four pilot countries (country boundaries delineated from ESRI Data and Maps). DEMs and tile schema are tailored and produced using Interactive Data Language (IDL). Third, imagery from the NCCS archive is selected based on project criteria (based on satellite, month, sensor, or year) and create a shape-file footprint of all available imagery. Fourth, the footprints are broken into each specific tile and sub-tile and generate all potential sub-tile time series. The image sub-tile time series are scored to lastly begin mosaic generation (See Figure 1). Selecting mosaic images according to mosaic tools scoring algorithm that uses metadata information to score each image based on its suitability. The variables used are cloud cover (lower is preferred), sun elevation (higher is preferred), off nadir angle (lower is preferred). The score is computed from Score = 48 * (1 - CloudCoverPercent) + 28 * (SunElev/90) + 24 * (90 - OffNadirAngle)/90.0. For the four pilot countries the following two continuous data extents were given (Figure 1): a) Senegal: (12°N - 17°N latitudes, 18°W - 6°W longitudes, spanning UTM 28N and 29N) and b) Uganda, Kenya, and Tanzania: (5°N - 12°S latitudes, 24°E - 42°E longitudes, spanning UTM 35N/S, 36N/S and 37N/S).

Updated guidelines on NextView Licensed imagery is that georeferenced images are allowed to be distributed, however no publicly released imagery can be reverse engineered to obtain the original image values, and each image must have a copyright burned into it. Furthermore, each public-ally released NextView derived image must receive approval from an appointed NGA/NextView reviewer. This is an additional requirement placed upon all projects using NextView Licensed imagery. To assist in conforming to the technical requirements of NextView License imagery, a number of automated scripts were developed which clip regions of interest from collections of the image archive (both mosaics and raw imagery), stitch them together, and finally burn in a copy right notice. It was decided in meetings with CI to use georeferenced "lossy" JPEG's as the distribution format ensuring conformance with NextView's requirement that the original images cannot be derived or reverse engineered.

A.1 PANCHROMATIC ONLY MOSAICS

From the beginning of the project, we have been tailoring the mosaic code to produce panchromatic only 50cm commercial high-resolution mosaics using all available data in order to reduce data gaps within the mosaics (years 2002 to 2016). The panchromatic mosaics are created from high-resolution imagery from GeoEye-1, QuickBird-2, WorldView-1, and WorldView-2. Mosaics include imagery that contains 20% or less cloud cover, includes all years and months, and only basic product codes P1BS and P4AM. Once mosaics were complete over Senegal, mosaics were reviewed for quality assurance (September 2016). Over 55,000 commercial satellite images were used to complete the panchromatic mosaic over Senegal (see Figure A1). Since mosaics came from different sensors and time, a contrast correction based on median histogram enhancement was applied (see figure A2).

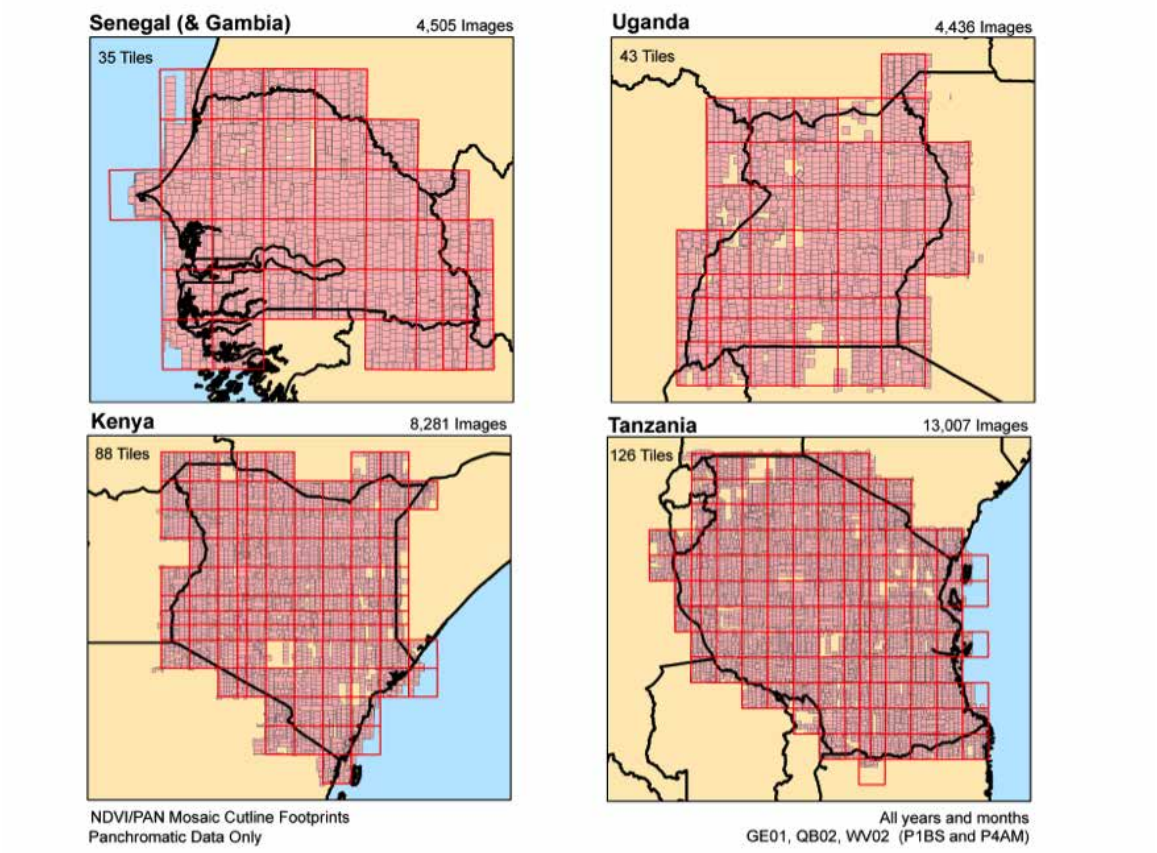

Figure A1. VHR mosaic tiles and image footprints for PAN images from NDVI/PAN mosaics.

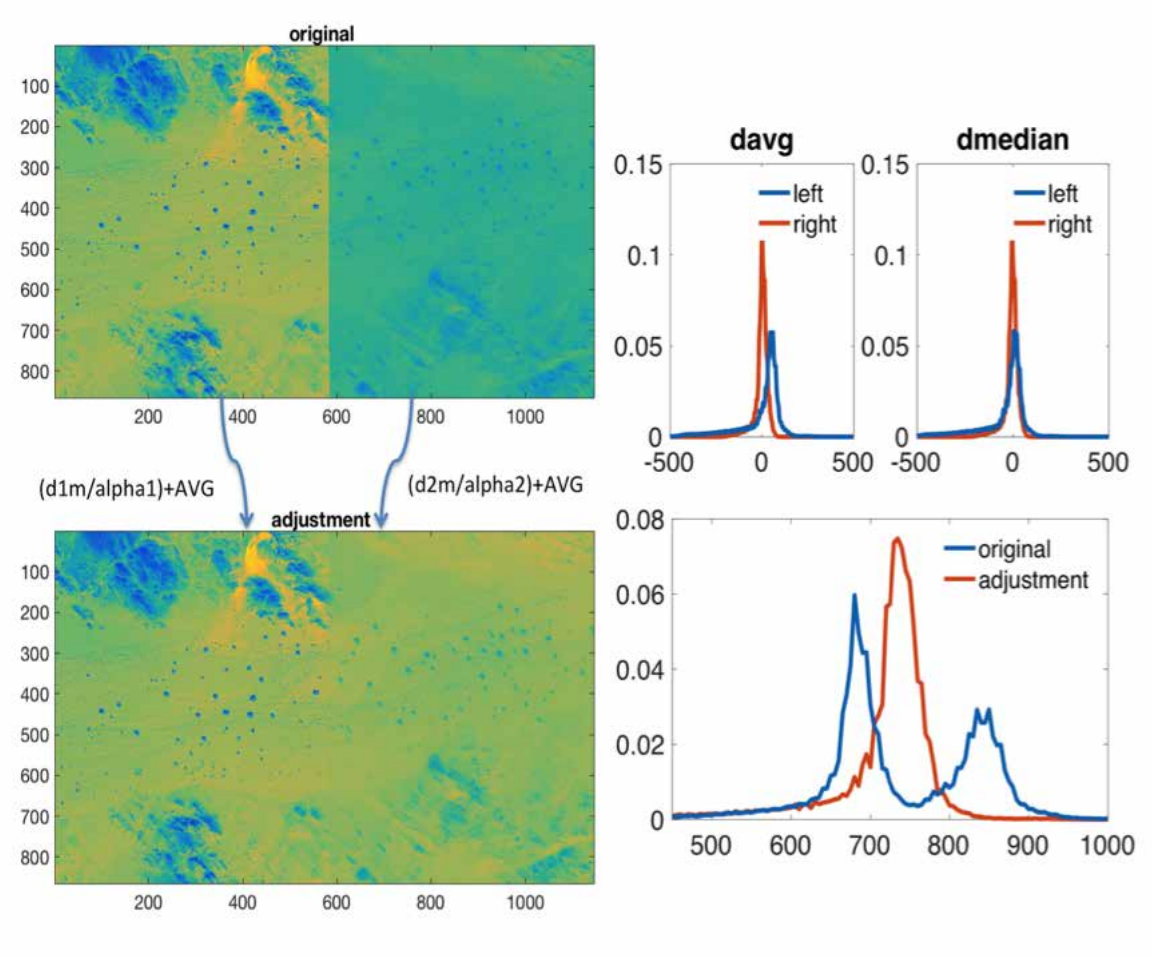

Figure A2. VHR mosaic tiles and image footprints for PAN images from NDVI/PAN mosaics.

A.2 NDVI/PAN MOSAICS

The NDVI/PAN mosaics are created from high-resolution imagery archive on NCCS from GeoEye-1, QuickBird-2, WorldView-1, and WorldView-2. Mosaics include imagery that contains 20% or less cloud cover, includes all years and months, and only product codes M1BS, M4AM, P1BS and P4AM. Over 188,000 VHR images in the archive are being used to select the ones that complete mosaics over the four pilot countries. Figure A2 shows the NDVI/PAN mosaic tiles and their commercial satellite image coverage.

Mosaics were generated over entire countries; however, to start other parts of the project mosaics were prioritized to get tiles surrounding 19 CI-VS and Lund University (LU) landscapes (shapefile provided by CI-VS and LU collaborators). There are 1,177 VHR images that directly intersect with the CI-VS sites and 25 100 x 100 km tiles that contains LU landscapes.

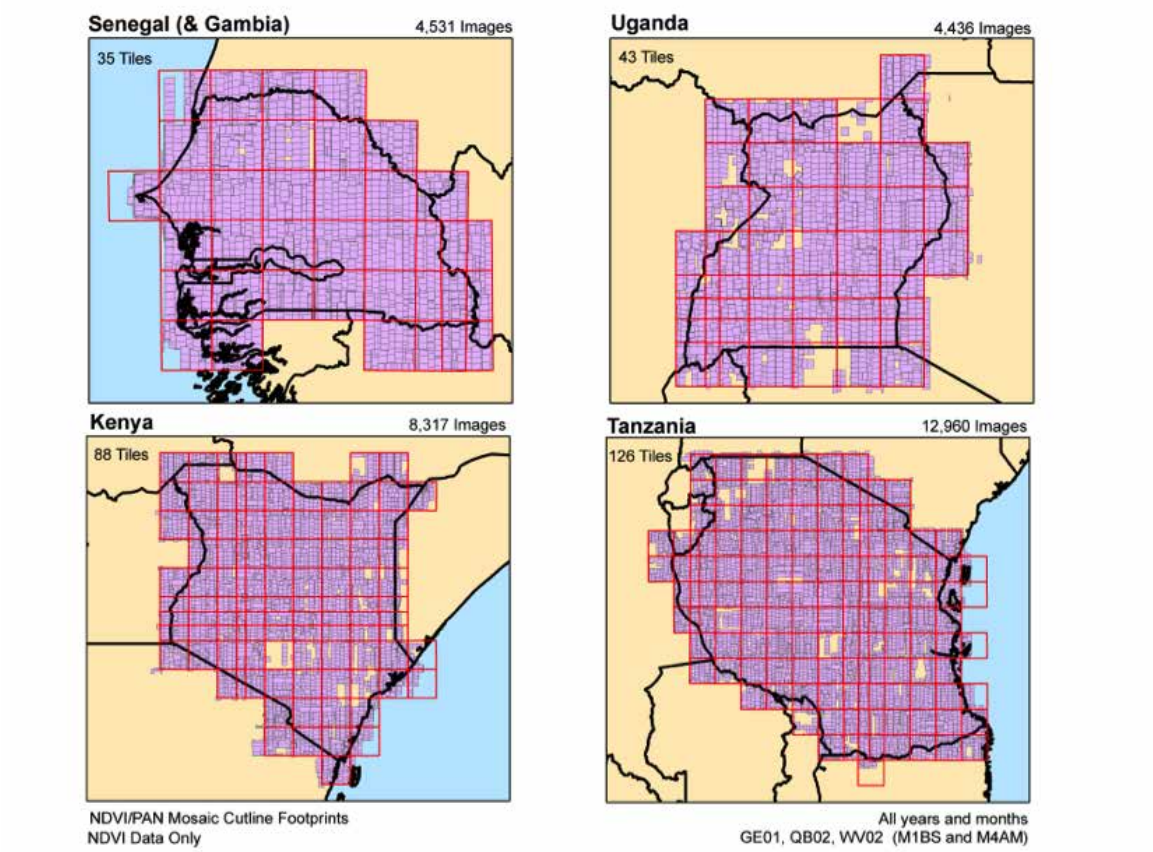

Figure A3. Commerical high resolution mosaic tiles and image footprints for NDVI/PAN mosaic.

APPENDIX B. COMMERCIAL VERY HIGH RESOLUTION MOSAICS

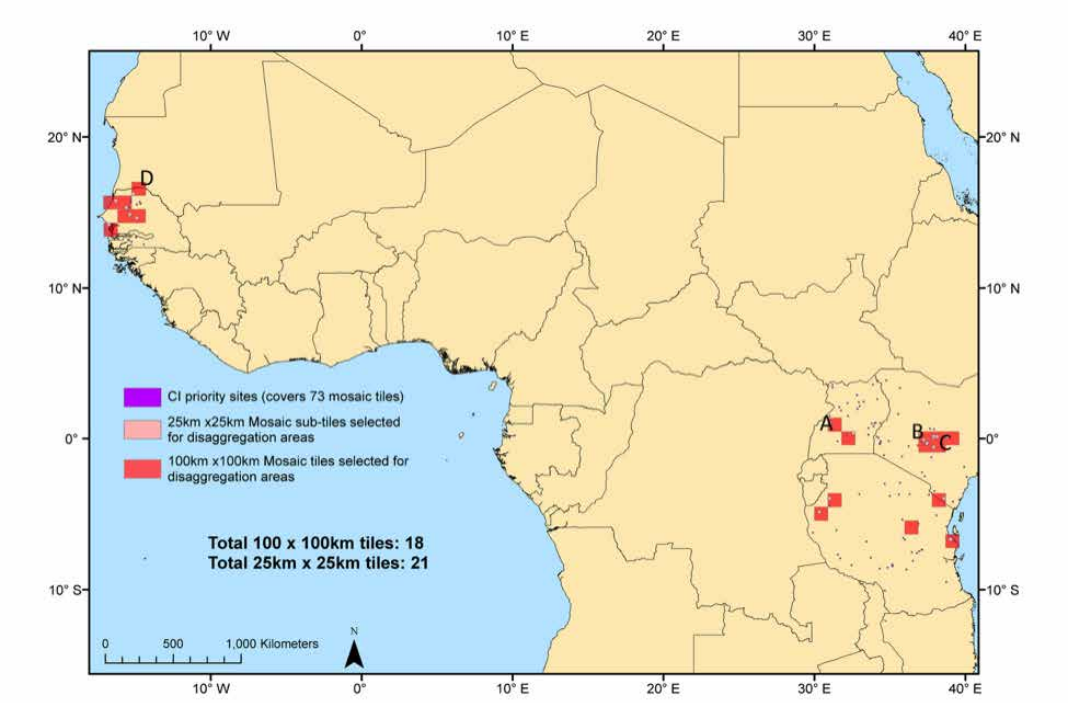

Figure B1. CI Priority sites and tiles selected for disaggregation. Regions A, B, C and D were studied in detail in main text.

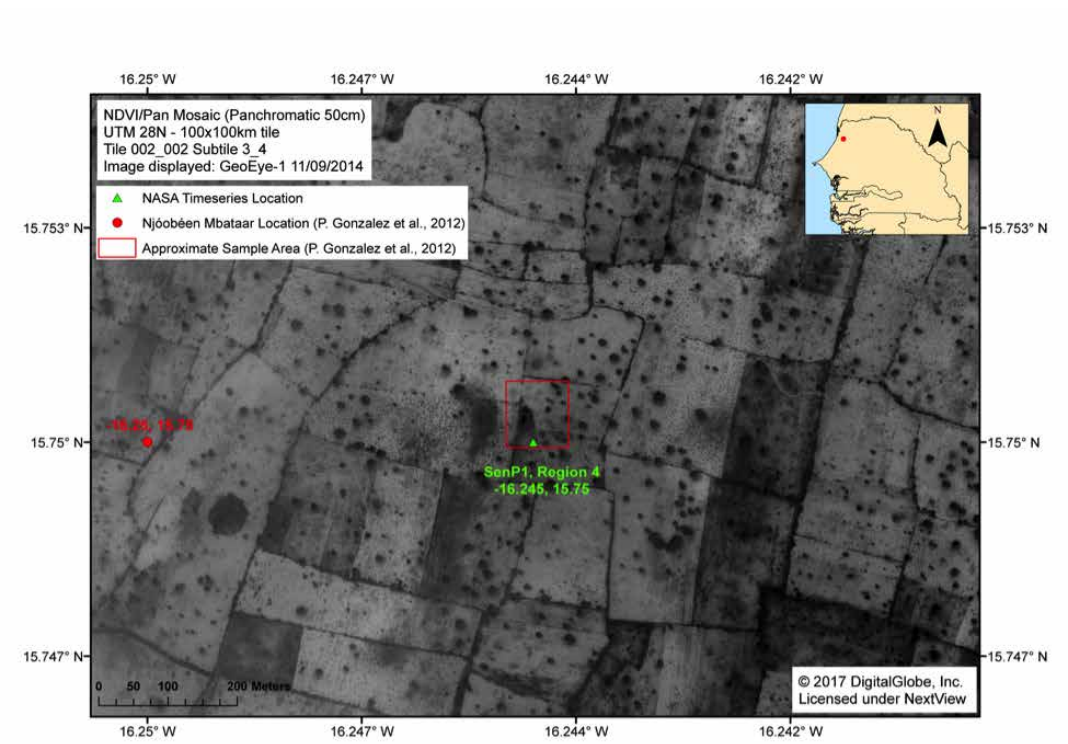

Figure B2. Zoom of DigitalGlobe image for current tree distribution. Region in squared-red represents the same region where Gonzalez *et al*. (2012) study where focused.

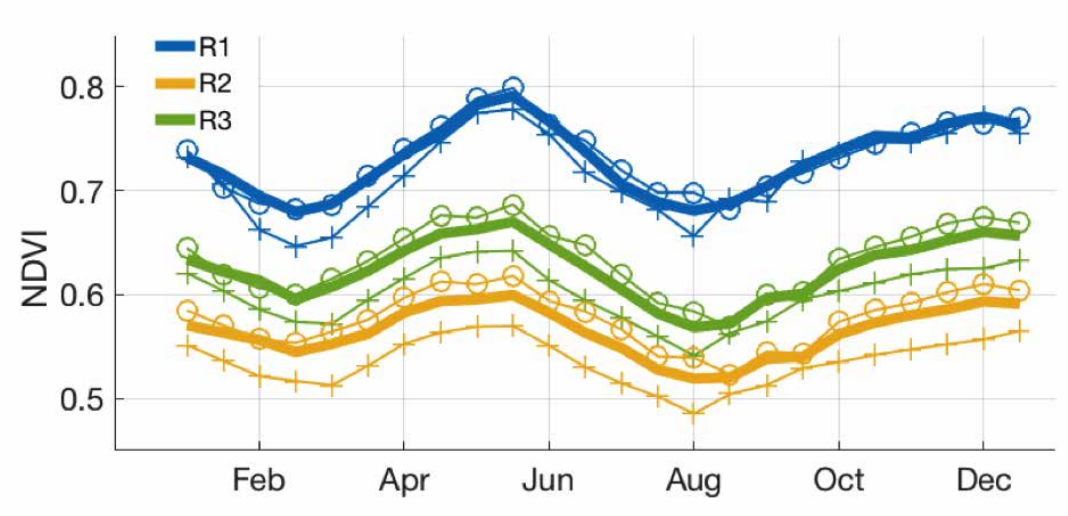

Figure B3. Decadal NDVI climatology (monthly average of NDVI during 10 years) that corresponds to regions R1, R2 and R3 in Uganda: Circles are (1990s climatology) and pluses (2000s climatology), and bold line 30-year climatology. Notice the convergence in climatology for R1 but the decreasing from 1990s to 2000s in R2 and R3.

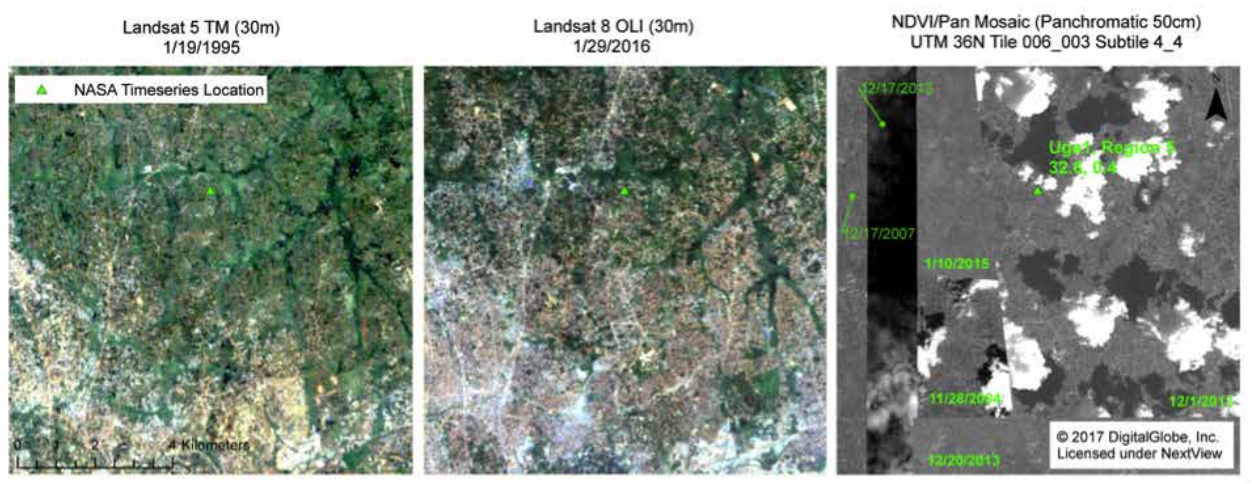

Figure B4. Dates of Landsat imagery and VHR mosaic data that are available for Uganda regions R1-R4 (See Figure 4).

PARQUE NACIONAL CHAPADA DOS VEADEIROS, CERRADO, BRAZIL.
CONSERVATION INTERNATIONAL/PHOTO BY STERLING ZUMBRUNN

CONSERVATION INTERNATIONAL

gef
GLOBAL ENVIRONMENT FACILITY
INVESTING IN OUR PLANET

VITAL SIGNS

LUND UNIVERSITY

NASA